The Company of **Biologists**

RESEARCH ARTICLE

Capillarity and active cell movement at mesendoderm translocation in the *Xenopus* gastrula

Martina Nagel[1], Debanjan Barua[1], Erich W. Damm[1,*], Jubin Kashef[2,‡], Ralf Hofmann[2,3], Alexey Ershov[2], Angelica Cecilia[2], Julian Moosmann[4], Tilo Baumbach[2] and Rudolf Winklbauer[1,§]

ABSTRACT

During *Xenopus* gastrulation, leading edge mesendoderm (LEM) advances animally as a wedge-shaped cell mass over the vegetally moving blastocoel roof (BCR). We show that close contact across the BCR-LEM interface correlates with attenuated net advance of the LEM, which is pulled forward by tip cells while the remaining LEM frequently separates from the BCR. Nevertheless, lamellipodia persist on the detached LEM surface. They attach to adjacent LEM cells and depend on PDGF-A, cell-surface fibronectin and cadherin. We argue that active cell motility on the LEM surface prevents adverse capillary effects in the liquid LEM tissue as it moves by being pulled. It counters tissue surface-tension effects with oriented cell movement and bulges the LEM surface out to keep it close to the curved BCR without attaching to it. Proximity to the BCR is necessary, in turn, for the maintenance and orientation of lamellipodia that permit mass cell movement with minimal substratum contact. Together with a similar process in epithelial invagination, vertical telescoping, the cell movement at the LEM surface defines a novel type of cell rearrangement: vertical shearing.

KEY WORDS: *Xenopus*, X-ray tomography, Gastrulation, Cell migration, Surface tension

INTRODUCTION

Mass cell migration positions organ rudiments during development. In the *Xenopus* gastrula, the leading edge mesendoderm (LEM) moves from the equatorial region as a coherent cells mass along the ectodermal blastocoel roof (BCR) to beyond the animal pole of the embryo (Nieuwkoop and Florschutz, 1950; Keller, 1976). Its mesodermal component contributes to the vascular system (Tracey et al., 1998); the endodermal part to the gut (Bouwmeester et al., 1996; Jones et al., 1999; Zhang et al., 2016). During their advance, LEM cells facing the BCR extend lamellipodia and underlap each other in the direction of movement, generating a distinctive 'shingle arrangement' (Winklbauer and Nagel, 1991; Nagel and Winklbauer, 1999). Guidance cues orienting the lamellipodia are provided by PDGF-A (Nagel et al., 2004) which is secreted by the

BCR and sensed by the PDGFR-α receptor of LEM cells (Ataliotis et al., 1995; Damm and Winklbauer, 2011). Moreover, an extracellular matrix of fibronectin (FN) fibrils on the BCR (Nakatsuji et al., 1985; Winklbauer, 1998) allows LEM cells to extend lamellipodia and migrate on explanted BCR (Winklbauer, 1990; Winklbauer and Selchow, 1992). These findings are consistent with PDGF-A-guided collective LEM migration on the BCR surface.

This proposition has been challenged by observations that the LEM is often separated from the BCR during movement (Moosmann et al., 2013; Sonavane et al., 2017). It raises the questions of how underlapping lamellipodia form away from the FN-coated BCR and what role these locomotory organelles play when not in contact with the supposed substratum. We show that non-fibrillar, punctate cell-surface FN (csFN) (Nagel and Winklbauer, 2018) and cadherin support the extension of lamellipodia on the surface of LEM cells. We argue that the ensuing cell-on-cell migration allows the wedge-shaped, yet liquid-like, LEM cell mass (David et al., 2014; Winklbauer and Parent, 2016) to move across the BCR while being mainly attached to the substratum at its tip: the shingle arrangement of oriented cells prevents capillary retraction or break up and the collapse of the LEM under its surface tension.

RESULTS

LEM cell protrusions extend on the surface of adjacent LEM cells

In the *Xenopus* gastrula, the advancing dorsal LEM forms an asymmetrical wedge with a concave blastocoelic surface and a convex surface that conforms to the BCR, and with large cells on the blastocoelic side and the front, and smaller cells further back on the BCR side (Fig. 1A-D). It invariably touches the BCR with its tip, while, further behind, it is attached or detached to varying degrees (Fig. 1A-D; Table S1). Directly behind the tip cell, a gap stretches over one to four cells in half of the specimens. Behind this front region, a continuous cleft is seen in one quarter of cases, while the other cases show full or sporadic BCR contact at the rear (Fig. 1C,D; Table S1). Time-lapse X-ray phase-contrast microtomography (TXPCµT) (Moosmann et al., 2013) reveals that LEM-BCR contact changes over a time scale of tens of minutes, explaining gap variability by dynamic contact behavior (see Fig. 6A; Table S1).

Despite being separated for prolonged times from the FN-rich BCR, most LEM cells extend filopodia and lamellipodia (Fig. 1E-I). Cells underlap each other in a shingle arrangement with lamellipodia (Winklbauer and Nagel, 1991), but also with the cell bodies and in the absence of protrusions (e.g. Fig. 1H,I). Some lamellipodia extend at gaps between LEM cells and could be supported by the BCR (e.g. Fig. 1G,H), while others appear attached to adjacent LEM cells (Fig. 1G). This is particularly

[1]Department of Cell and Systems Biology, University of Toronto, Toronto M5S 3G5, Canada. [2]Karlsruhe Institute of Technology, 76021 Karlsruhe, Germany. [3]Institut für Theoretische Physik, Universität Heidelberg, 69120 Heidelberg, Germany. [4]Helmholtz-Zentrum Geesthacht, Zentrum für Material- und Küstenforschung, 21502 Geesthacht, Germany.
*Present address: Department of Biology, Virginia Commonwealth University, Richmond, VA 23284-2012, USA. ‡Present address: STRATEC SE, Birkenfeld 75217, Germany.

§Author for correspondence (r.winklbauer@utoronto.ca)

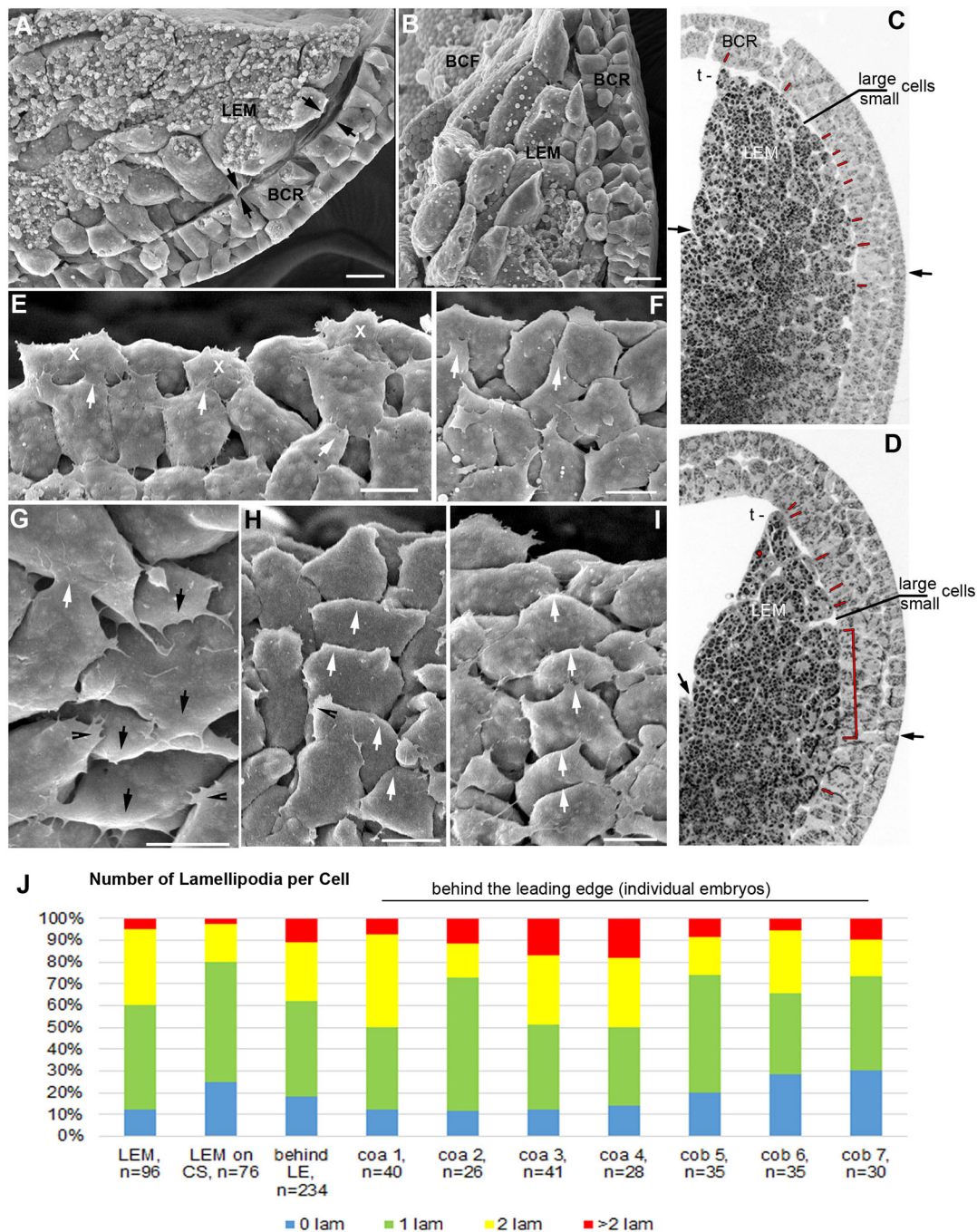J.K., 0000-0002-0085-4634; R.W., 0000-0002-0628-0897

DEVELOPMENT

1

Fig. 1. Cell arrangements in the LEM. (A,B) Sagittally fractured mid-gastrulae under a scanning electron microscope. Brachet's clefts of variable width (between opposing arrows) separate the LEM from the BCR (*n*=31). (C,D) Histological sections of mid-gastrulae. The LEM forms a wedge between the level of arrows and tip cells (t). Contact with BCR is indicated by the red dashes or bracket (*n*=24). (E-I) Mid-gastrula LEM seen from the BCR side (*n*=21). (E,F) Front region with tip cells alternatingly extending protrusions (x). Lamelliform protrusions in tiers behind tip cells appear closely attached to the cells ahead (white arrows). (G-I) LEM cells further behind show cell-surface attached (white arrow in G) and free lamellipodia (black arrowheads), filiform processes and chains of cells that underlap animal-vegetally (white arrows in H,I) with cell bodies with or without protrusions (H,I). Occasionally, direction of underlapping is reversed locally (black arrows in G). (J) The number of lamellipodia per cell, seen as protrusions flattened at least at their ends in the plane of the LEM surface [n, number of cells examined; columns 1 and 3 are from seven embryos per bar; column 2 is for conditioned substratum (CS) from four embryos; remaining columns are from single embryos each]. Scale bars: 30 µm.

obvious directly behind the tip, where cells are often detached from the BCR (Fig. 1E,F). The number of lamellipodia per cell is comparable between this region and the whole LEM (Fig. 1J). These observations suggest that LEM lamellipodia can extend on the BCR surface, but also on the substratum-facing surface of other LEM cells.

The protrusive activity of LEM cells on non-adhesive bovine serum albumin (BSA) confirms this notion (Fig. 2). Single cells remain round and aggregates do not spread due to the absence of marginal lamellipodia (Fig. 2A,B), in contrast to aggregates on FN (Fig. 2C). Sub-marginally, small protrusions form but retract rapidly (Fig. 2E) due to contact inhibition that can be overcome by
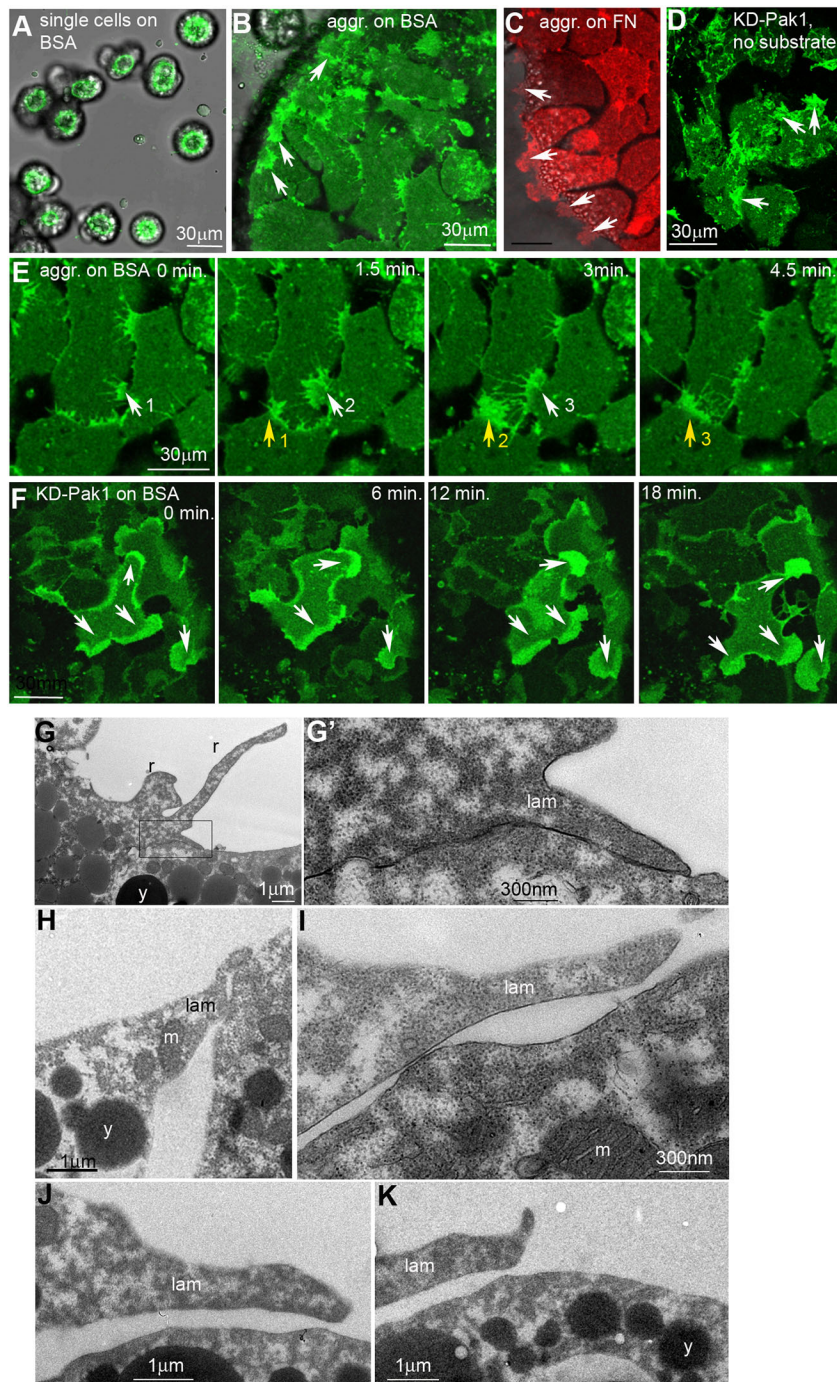
Fig. 2. LEM lamellipodia on LEM cell surface.
(A-F) Explants labeled with membrane-GFP (A,B,D-F) or AlexaFluor488-phalloidin (C) to visualize lamellipodia (arrows). On non-adhesive bovine serum albumin (BSA) or on the free surface of aggregates, lamellipodia can form only on other LEM cells (A,B,E; n=11; two experiments; D,F; n=9; two experiments). On FN substratum, lamellipodia extend from the margin (C; n=8; two experiments). Expression of kinase-dead Pak1 stabilizes and enlarges lamellipodia (D,F). (E,F) Frames from time lapse recordings. Two different lamellipodia (yellow and white arrows, respectively) were followed through three consecutively numbered time points each.
(G-K) Transmission electron micrographs of lamellipodia at the surface of LEM explants expressing kinase-dead Pak1 (n=3). r, membrane ruffles; y, yolk platelets; m, mitochondria; lam, lamellipodia. Scale bars: 30 µm in A-F; 1 µm in G,H,J,K; 300 nm in G,I.

expression of a kinase-dead p21-activated kinase1 (Pak1) (Nagel and Winklbauer, 2018). In aggregates on BSA, LEM cells expressing this KD-Pak1 construct extend large, long-lived lamellipodia that move on the surfaces of adjacent cells (Fig. 2F). Protrusions form also on the upper surface of aggregates completely devoid of interaction with an external substratum (Fig. 2D).

KD-Pak1-induced lamellipodia form different types of substratum contacts (Fig. 2G-K). They are frequently attached over their whole length through close 10 nm-wide contacts (Fig. 2G,G′), but they also make close contacts at points while being separated in between (Fig. 2H), or at an adherens junction-like contact at their base (Fig. 2I). Strikingly, lamellipodia and substratum can be separated by hundreds of nanometers (Fig. 2J,K), corresponding to the wide adhesive contacts previously identified at the mesoderm-ectoderm interface (Luu et al., 2015).

csFN and cadherin are required for lamellipodia formation on LEM cell surfaces

Xenopus endoderm cells require interaction with csFN and C-cadherin for cell-on-cell migration (Wen and Winklbauer, 2017), and LEM lamellipodia also depend on these factors. Knockdown of FN in KD-Pak1-expressing LEM explants (Fig. 3A) abolishes the increase in lamellipodia frequency caused by KD-Pak1 (Fig. 3E), and the broad lamellipodia are reverted to those of controls. They extend from a narrow base at the cell margin,
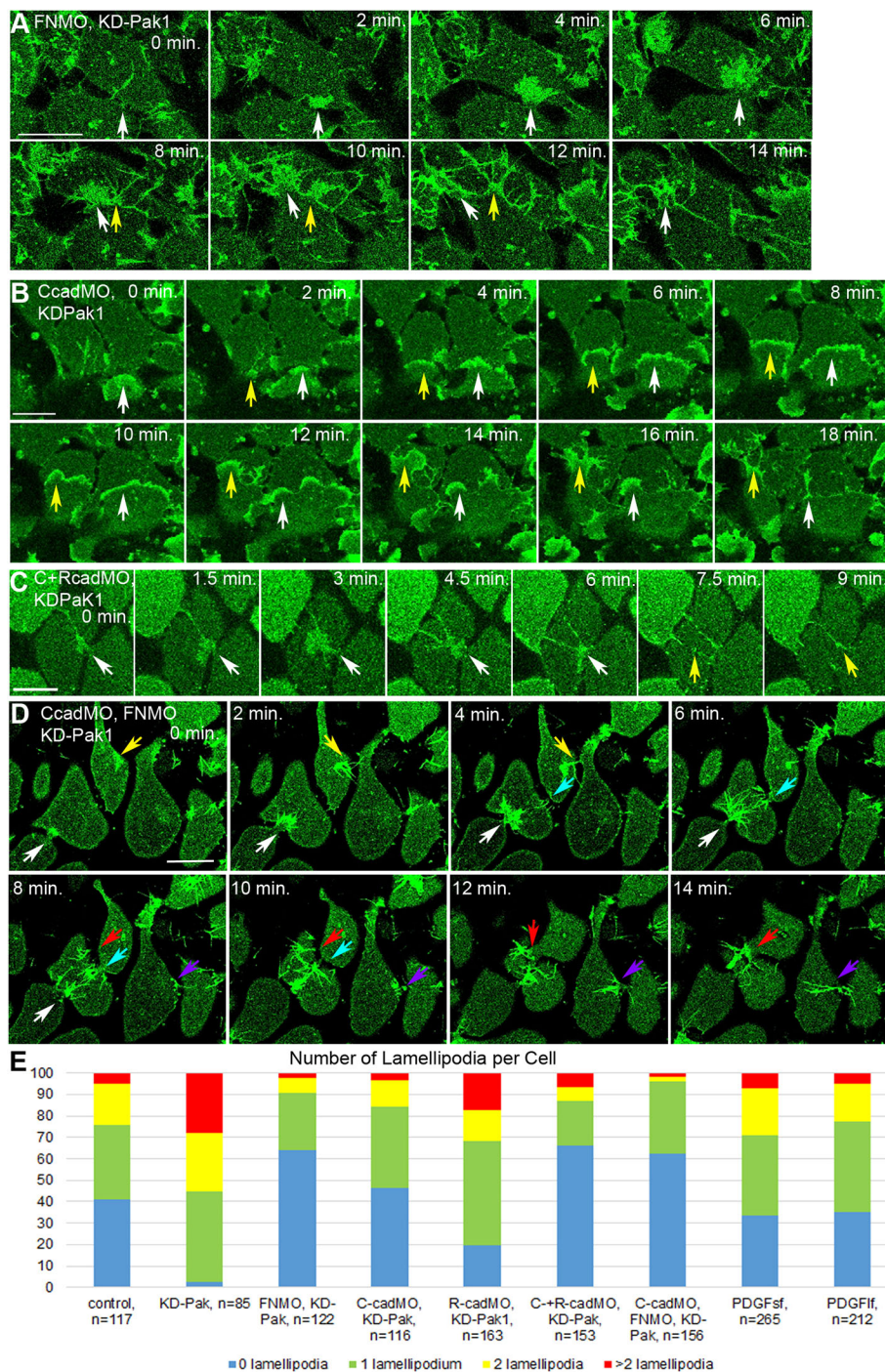
Fig. 3. Fibronectin and cadherin requirements for LEM lamellipodia. (A-D) Time-lapse recorded KD-Pak1/membrane-GFP-expressing LEM explants co-injected with FN-MO (A) (*n*=14; 2 experiments), C-cadherin-MO (B) (*n*=11; 2 experiments), a mix of C- and R-cadherin MOs (C) (*n*=10), and a mix of C-cadherin and FN MOs (D) (*n*=10; 2 experiments). Frames after indicated times of recording are shown. Individual lamellipodia (arrows) are followed. Scale bars: 30 µm. (E) Number of lamellipodia per cell as seen in the time-lapse recordings (*n*, number of cells examined; each column shows data from five movies; cells were evaluated in one representative frame in each movie).

move rapidly across cell surfaces, and collapse into filiform processes that accumulate as retraction fibrils (Fig. 3A; Fig. S1A,B). When cells move apart, connecting fibrils are ruptured instead of detaching (Fig. S1A), whereas detachment occurs in retracting lamellipodia of DN-Pak1 explants (Fig. S1C). Thus, csFN is required for lamellipodia formation and for their orderly retraction on the LEM surface.

C-cadherin knockdown also reduces lamellipodia frequency; R-cadherin, a minor cadherin isoform in the gastrula (Tashiro et al., 1995), has only a mild effect (Fig. 3E). Interfering with both cadherins simultaneously (Fig. 3E) has an additive effect. Knockdown of csFN or C-cadherin reduces expression of the respective proteins to one-third (Nagel and Winklbauer, 2018), consistent with residual lamellipodial activity. Co-inhibition of csFN and C-cadherin does not further reduce lamellipodia abundance (Fig. 3E), suggesting that the factors act non-additively. Lamellipodia resemble those of Pak1-inhibited cells when C-cadherin is knocked down alone (Fig. 3B). However, when both cadherins are co-inhibited, or C-cadherin is inhibited together with csFN, they resemble those of csFN morphants, and retraction fibers persist (Fig. 3C,D; Fig. S1D). Thus, csFN and cadherins have similar roles but are both required, as if acting in a single pathway.

To detect csFN and C-cadherin on the LEM surface, embryos were fixed immediately after removal of the BCR and stained using
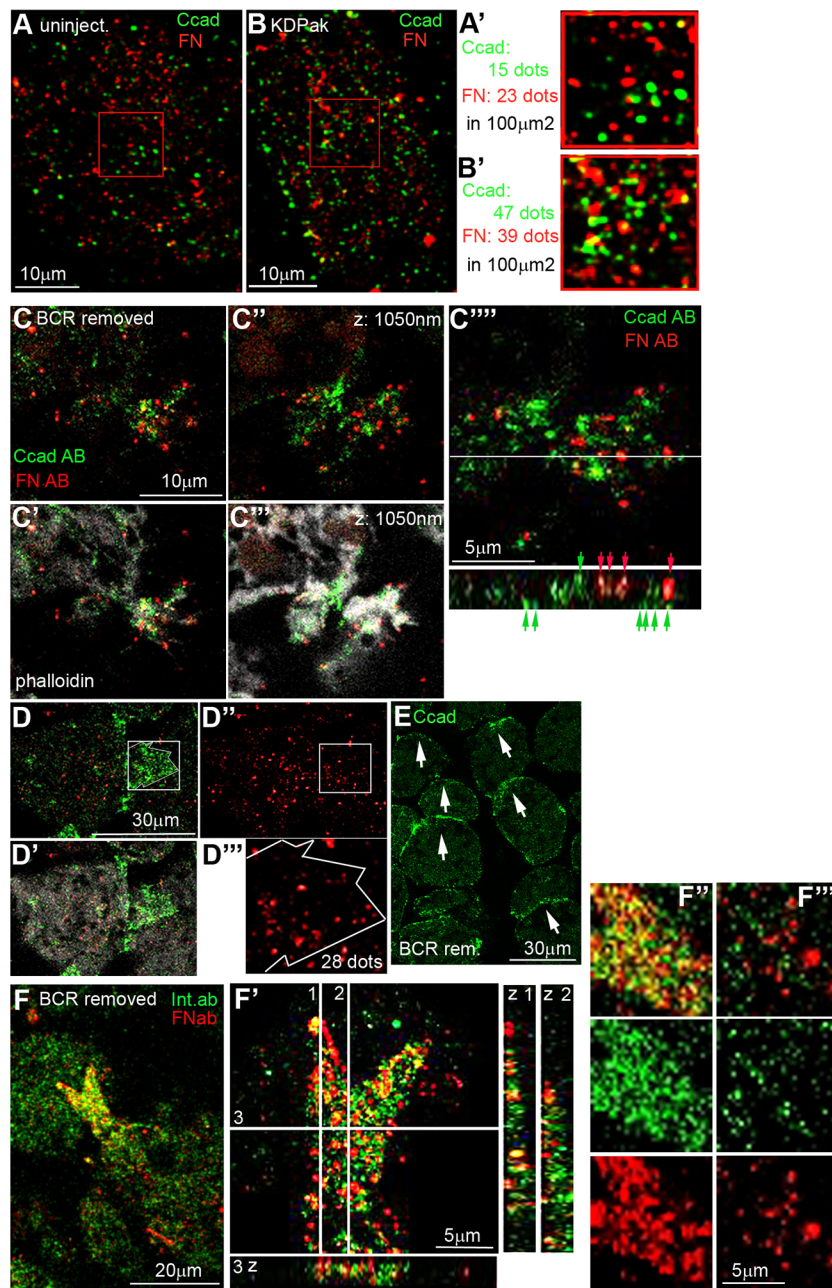
Fig. 4. csFN and C-cadherin puncta on LEM cells.
(A,B) The BCR-facing surface of untreated (A) (*n*=26; 2 experiments) and KD-Pak1-expressing LEM (B) (*n*=12; 2 experiments) stained after BCR removal for FN (red) and C-cadherin (green). Puncta were counted in the boxed areas (higher magnification in A′,B′). (C-E) Protrusion-bearing LEM cell surfaces triple-stained using FN antibody (red), C-cadherin antibody (green) and fluorescent phalloidin (white) (*n*=12; 2 experiments). Planes at the free surface (C,C′) and at the undersurface near the substratum (C″,C‴), and a z-projection (C‴′) show C-cadherin puncta underneath and at the free surface of protrusion (green arrows in C‴′); csFN puncta occur mostly at the free surface (red arrows in C‴′). A C-cadherin-rich protrusion (D,D′) covers non-accumulating csFN puncta (D″,D‴). (E) C-cadherin at animally pointing (arrows) cell edges. (F) Protrusion-bearing LEM cell surfaces double stained for FN (red) and integrin β1 (green) (*n*=18; 2 experiments). Dashed lines outline the cell bodies. (F′) Z-plane projections (0.346 μm×7) show accumulation of csFN puncta at the free surface. Higher magnifications of the protrusion (F″) and a cell body (F‴), with merged (top), integrin (middle) and FN (bottom) channels showing partial colocalization. Scale bars: 10 μm in A-C‴′; 30 μm in D-E; 20 μm in F; 5 μm in F′-F‴.

antibodies (Fig. 4A; Fig. S2A,A′). csFN forms micrometer-sized puncta. Their density in the range of 0.1 to 1 FN puncta/μm² is sufficient to support lamellipodia (Zimmerman et al., 2017), although FN is more abundant in the matrix of the BCR (Fig. 4C; Fig. S2C,C′). Cadherin puncta are similarly spaced but rarely overlap with csFN (Fig. 4A). When fixed 30 min after BCR removal (Fig. S2B,B′), csFN and cadherin puncta have become coarse. KD-Pak1 does not alter the pattern of csFN or cadherin puncta except for an increase in cadherin density (Fig. 4B; Fig. S2D-F′). Thus, both adhesion molecules are consistently present on the LEM surface.

LEM lamellipodia interact with csFN and cadherin puncta (Fig. 4D,E). C-cadherin is enriched at both substratum-apposed and free surfaces of lamellipodia and csFN preferentially on free surfaces (Fig. 4D,D′). Cells also increase C-cadherin density at their animal side in the absence of lamellipodia (Fig. 4F). Adhesion to C-cadherin *in vitro* is sufficient to induce lamellipodia in LEM cells

(Fig. S4), and some lamellipodia show only cadherin and no csFN enrichment (Fig. 4E), but for cadherin to act as substratum, only a fraction of LEM protrusions would be sufficiently close to the cell surface. csFN does not co-localize with integrinβ1 puncta, except at lamellipodia where csFN and integrinβ1 are highly enriched (Fig. 4F′-F‴; Fig. S3A-C). csFN puncta may be carried forward with the advancing protrusions, perhaps bound to diffuse integrinβ1-containing receptors and serving a signaling role on the upper surface of lamellipodia.

Role of PDGF-A in lamellipodia stabilization on LEM cell surfaces
Secretion by the BCR of a diffusible short-form sf-PDGF-A (Mercola et al., 1988; Damm and Winklbauer, 2011) promotes LEM lamellipodia (Nagel et al., 2004; Nagel and Winklbauer, 2018). To see how lamellipodia depend on proximity to the BCR, we removed
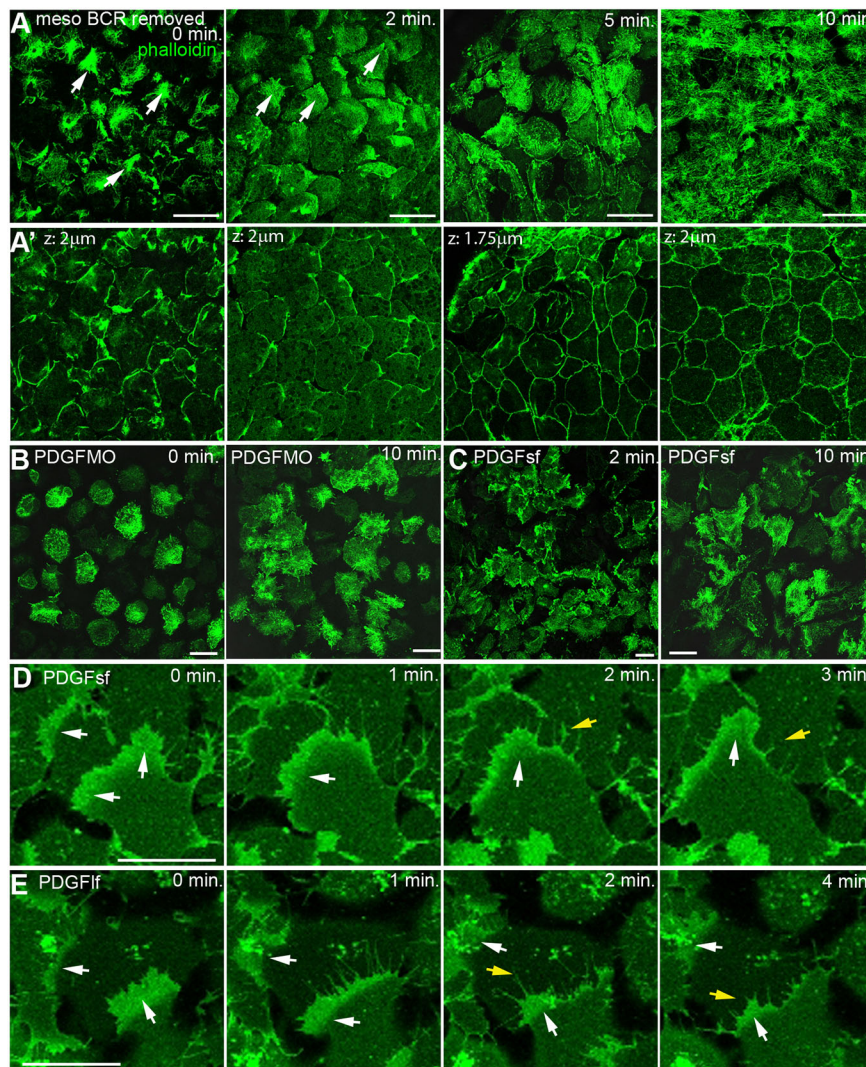
Fig. 5. BCR-dependent F-actin patterns in LEM.
(A-C) F-actin (fluorescent phalloidin) of the BCR side of LEM fixed at various times after BCR removal. Untreated LEM (A) (n=15; 3 experiments) with oriented protrusions (white arrows) or at up to 2 μm depth in tissue (A′). (B,C) F-actin pattern when PDGF-A is knocked down in the BCR (PDGFMO) (B) (n=16; 2 experiments) or diffusible short-form PDGF-A is overexpressed in the BCR (PDGFsf) (C) (n=10; 2 experiments). (D,E) Time-lapse recordings of LEM explants on BSA expressing membrane-GFP and short-form PDGF-A (D) (n=6; 2 experiments) or cell surface-binding long-form PDGF-A (PDGFlf) (E) (n=3). Lamelliform protrusions (white arrows) and retracting fibrils (yellow arrows) are indicated. Scale bars: 30 μm.

the BCR from embryos that were then fixed after various times (Fig. 5A,A′). When fixed immediately, F-actin is concentrated in protrusions on the LEM surface. After 2 min, a meshwork of fine F-actin fibrils appears on cell bodies, and protrusions become small and rare. After 5-10 min, protrusions have disappeared, and a cortical F-actin meshwork covers the LEM surface (Fig. 5A,A′).

In PDGF-A morphants, the F-actin pattern immediately after BCR removal resembles that of long-term BCR-deprived embryos (Fig. 5B). Conversely, adding PDGF-A counters the effects of lasting BCR removal: when sf-PDGF-A is expressed in the LEM, cells still show protrusions when fixed 2 min after BCR removal. However, protrusions disappear and a fibrillar cortex develops when BCR has been absent for 10 min (Fig. 5C), probably due to secreted sf-PDGF-A escaping into the medium. Indeed, when sf-PDGF-A or cell surface binding long-form lf-PDGF-A-expressing aggregates are placed under a coverslip (Fig. 5D,E), large KD-Pak1-type lamellipodia form at numbers resembling those in the embryo (Fig. 1N), and retraction fibers detach smoothly (Fig. 5D,E). Thus, BCR-secreted PDGF-A is necessary and sufficient to control LEM lamellipodia. Transient clefts formed between LEM and BCR seem sufficiently small to allow diffusible sf-PDGF-A to continuously promote cell motility on the LEM surface.

Movement of the LEM on a moving BCR substratum

To understand the role of persistent oriented protrusions in cells regularly detaching from external substratum, we examined LEM translocation in the opaque *Xenopus* gastrula by TXPCμT (Moosmann et al., 2013). First, we analyzed LEM-BCR contact dynamics (Fig. 6A; Table S1). Frequencies of contact types – full separation, full contact, and a mixture of contacting and separated interface – matched those in the SEM data. In front and in rear regions, full contact was seen half of the time. Contact varied independently in both regions and between planes about two cell diameters apart, indicating that attachment and detachment are localized to small cell groups. From nine images obtained at 10 min intervals, an upper bound for the duration of contact episodes was estimated as 10-15 min for separation, and 15-20 min for full or mixed contact (Table S1).

Next, we defined the context of LEM movement (Fig. 6A). As BCR and blastopore move vegetally during epiboly, mesoderm involutes at the blastopore lip and moves back animally inside the embryo, to turn again and insert itself at the mesoderm-BCR boundary (Winklbauer and Schürfeld, 1999; Ibrahim and Winklbauer, 2001). Below this 'insertion zone', internalized cells follow the blastopore lip vegetally; above it, cells translocate animally. As the BCR shifts vegetally at all points, the vegetally
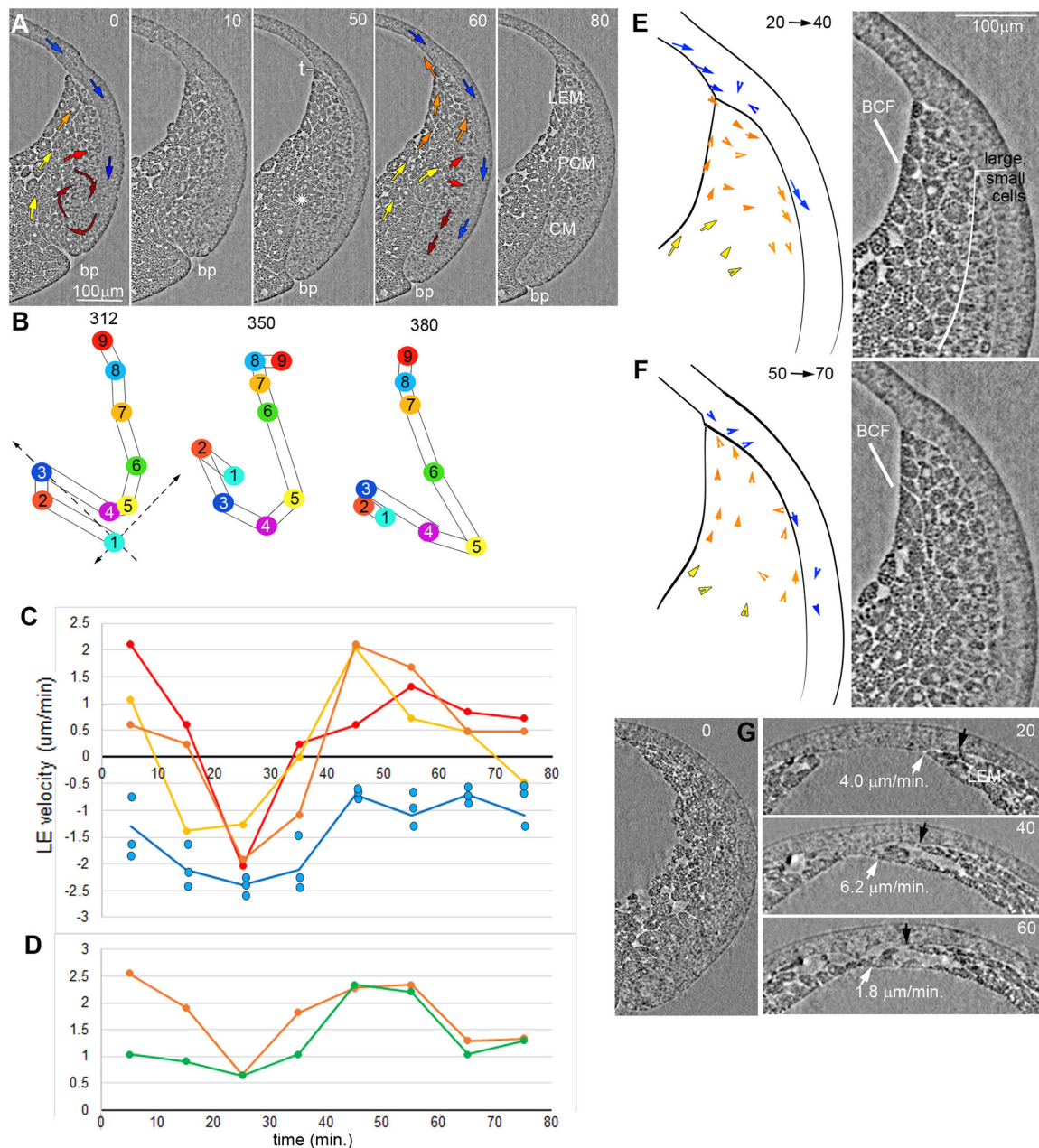
Fig. 6. TXPCμT analysis of LEM movement. (A) Select frames (0, 10, 50, 60 and 80 min) from recording in the mid-sagittal plane. BCR, blue arrows; endoderm of vegetal cell mass, yellow arrows; LEM, orange arrows; prechordal mesoderm, light-red arrows; chordamesoderm, dark-red arrows; bp, blastopore; star, anterior end of archenteron; t, tip cells. (B) Positions of tip cells at consecutive 10 min time points from the start (1) to end (9) of a movie in three parallel planes [planes 312, 350 (sagittal) and 380]. The dashed line pointing towards the top left parallels the tangent to the BCR surface at the level of the tip cell; the line perpendicular to this indicates the radial direction. (C) From B, tangential velocity components of the tip in the three planes (red, orange and yellow) were determined from BCR markers at the level of the LEM. The tangential component of epiboly is in blue. Animal direction is indicated by positive values. (D) Average velocity of LEM tip from C (orange line) is compared with the ratio of front-to-rear LEM attachment (green line). Values from Table S1 were multiplied by an arbitrary factor to adjust graphs to the same range. (E,F) Movements of cells between 20 and 40 min (E) and between 50 and 70 min (F). The final frame is shown (right) and the BCF layer is indicated. (G) Late gastrula LEM movement, 0 min frame showing dorsal side (left); 20, 40 and 60 min frames show animal pole region (right). The velocity of the tip cell (white arrows) is indicated; black arrows indicate BCR-attached LEM tip cell.

localized chordamesoderm moves in parallel with the BCR, whereas the animally situated LEM advances against the BCR movement.

These different conditions require different strategies of movement, as seen when BCR and underlying mesoderm are vitally stained in register with Nile blue sulfate (Kirschner and Hara, 1980). When the LEM is targeted, labels in the LEM and BCR become completely separated after 2 h (Fig. S5A). By contrast,

when chordamesoderm and adjacent BCR are labeled, the mesoderm patch is distorted but remains in broad contact with the BCR patch (Fig. S5B), which is confirmed when a fluorescently labeled plug of BCR and attached chordamesoderm is transplanted (Fig. S5C,D). Thus, chordamesoderm moves vegetally fastest at its contact with the still faster BCR, and slower in deeper layers, minimizing shear at the boundary by distributing it over its whole width. By contrast, the LEM moves as an essentially non-deforming
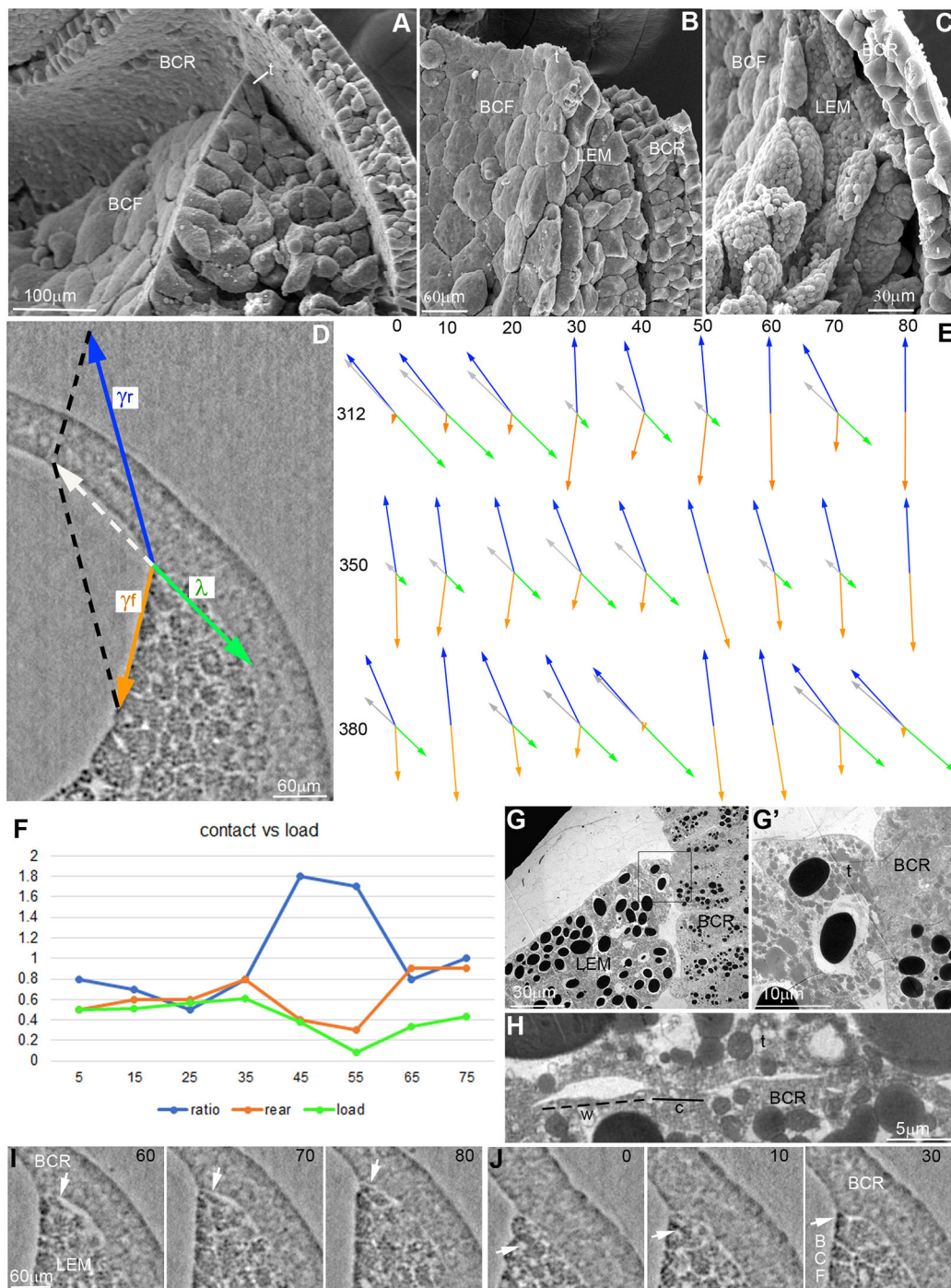
Fig. 7. Tip cells. (A-C) Sagittal fractures under a scanning electron microscope, with the BCF surface layer of LEM (*n*=31). (D) Tension balance at the LEM tip-BCR interaction. Blue, tension tangential to surface of cusp in BCR; yellow, tension at the BCF surface; green, load balancing, which is the result of tensions (white dashed arrow). (E) Tension balance diagrams for LEM tip-BCR attachments at different times (min) and planes (312, 350 and 380). (F) Load tension (green line, green vector arrows in E) follows the degree of BCR contact of the LEM rear region (orange line) (Table S1), but not the ratio of front-to-rear region contacts (blue). (G-H) TEM micrographs of tip cell-BCR contacts (*n*=12). (G′) Higher magnification of the region boxed in G. t, tip cell of LEM. (H) Alternation of close (c) and wide (w) contacts. (I,J) Exchange of tip cells by cells arriving from the BCR-facing surface of the LEM (arrows in I) or from the BCF surface (arrows in J).

cell mass relative to the BCR, and shear is concentrated at the boundary.

We followed the tip of the LEM in three planes about two cell diameters apart (Fig. 6B). During the interval recorded, the tip started in the animal direction, then fell back, but eventually progressed animally. LEM movement tangential to the BCR surface is with or against the BCR epibolic flow of 1-2 µm/min (see below).

Epiboly-related thinning of the BCR adds a normal component of 0.4 µm/min to the LEM movement. Movements are similar in the different planes, but not identical (Fig. 6B). To quantify translocation of the LEM tip, the tangential velocities of LEM tip and BCR cells were compared (Fig. 6C). LEM velocity is positive first, i.e. directed animally, but becomes negative before it suddenly turns positive again. The velocity of epiboly is always negative, but
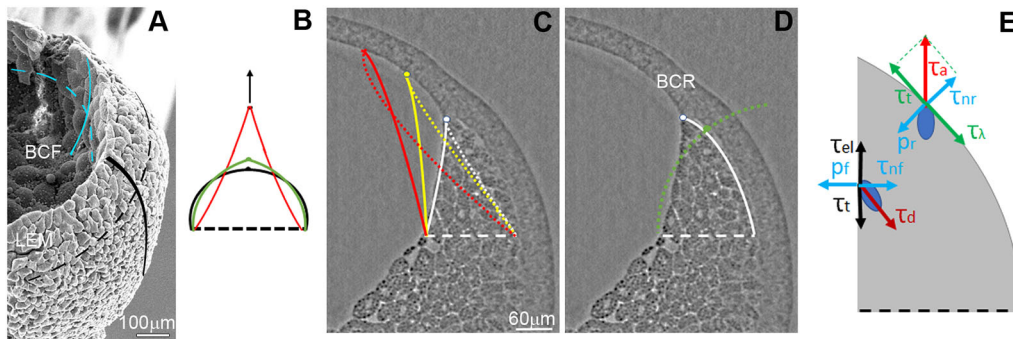
Fig. 8. Mechanical role of cell motility at LEM surface. (A) Scanning electron micrograph of the LEM wedge. Principal curvatures on BCR-apposed (black) and BCF (blue) sides, and along the perimeter (dashed) and the sagittal profile (solid lines). (B) Cross-sectional profile of liquid cylinder (black outline) attached to substratum (dashed line) being pulled (arrow) to assume wedge shape with convex (green) and then concave (red) minimal surfaces. (C,D) Actual LEM surfaces and surfaces predicted under various conditions. (C) Without adhesion to the BCR or oriented cell movement, curvature on a BCR-facing surface could equal that on the BCF side; curvature along the perimeter is neglected (solid and dotted white lines). To conserve volume, wedge height increases (yellow lines). If curvature along the perimeter is also considered, a further increase in LEM height is required (red lines). Solid and dotted lines cross over, suggesting fragmentation of the LEM. (D) Same scenario as in C, but a BCR-adjacent surface (white line) is applied to both sides (green dotted line). (E) Stress and pressure patterns due to active cell movement at the LEM wedge. p, Laplace pressure; τ, stress. Subscripts: r, BCR side of LEM; f, BCF side; n, normal; t, tangential; a, active shingle cell movement; λ, load; d, pulling of BCF cell; el, elasticity of BCF layer.

less so in the second half of the filmed interval. However, LEM velocity becomes positive before epiboly rate decreases. In fact, the velocity of the LEM relative to the BCR is not constant but decreases from 2.5 μm/min to 0.6 μm/min before it increases again (Fig. 6D).

This velocity variation matches the variable contact of the LEM to the BCR. After the first 20 min, relative velocity closely follows the ratio of front to rear contact (Fig. 6D; Table S1C). This ratio increases after 30 min by an increase in front contact, and then further by a sudden decrease in rear contact. After 60 min, rear contact increases again, reducing the ratio and hence the velocity. However, epiboly has slowed down and LEM movement remains positive, in contrast to an earlier phase where a similar LEM velocity led to negative net movement due to strong epiboly. Altogether, it appears that BCR adhesion at the front supports LEM translocation, rear attachment antagonizes it and the relative velocity determined by the balance of these effects leads to movement towards or away from the animal pole, depending on epiboly rate. Over the whole of gastrulation, the relative LEM velocity is 2.1 μm/min (Fig. S5E).

Changes in overall direction of movement are also seen at the cell level (Fig. 6E,F). Occasionally being pulled vegetally may explain rare examples (two out of our 31 specimens) of inverse shingle arrangement where cells are inclined vegetally instead of animally (Fig. S6). Animally directed net LEM translocation accelerates at later gastrula stages to reach 4-6 μm/min. The large cells of the blastocoel surface form a distinctive BCF layer of the LEM that can separate from the deeper cells migrating on the BCR, advance behind a tip cell riding on a moving BCR cusp and eventually fuse with the corresponding layer from the ventral side (Fig. 6G). This indicates that BCF layer and lead cells form a functional unit, and that rear LEM cells can migrate on the BCR when epiboly has become slow. Overall, adapting to epiboly, chordamesoderm remains firmly attached to the BCR and moves with it vegetally while the LEM regulates attachment of its subregions such that, in the long term, it moves animally faster than the BCR vegetally.

Tip cell – blastocoel roof interaction

The LEM tip cells always maintain contact with the BCR (Figs 1A-D, 7A). They are part of the BCF layer whose large tightly packed cells form a smooth surface (Fig. 7A,B). To the BCF layer, obliquely oriented deep cells are attached (Fig. 7A-C). At the tip

cell-BCR contact, the BCR forms a cusp (Moosmann et al., 2013) that immediately collapses when occasional tip cells detach spontaneously (Fig. S7E,F), or does not form when the LEM advance is impeded, e.g. by dnPDGF (Fig. S8B-D). The LEM rim likewise collapses immediately when the BCR is removed (Fig. 9A,B). Thus, the tip cell-BCR contact mediates mechanical interaction that can be characterized by a tension diagram (Fig. 7D).

Xenopus gastrula tissues exhibit surface and interfacial tensions of known magnitude (David et al., 2014; Luu et al., 2011). We assume a fixed tension at the free BCR surface, γ_r, based on its tissue surface tension and any residual elastic stresses, and similarly a tension for the BCF surface behind the tip cells, γ_f. The latter is transmitted to the BCR by the migratory tip cells. Its magnitude is constructed such that the component of γ_r in the direction of movement tangential to the BCR is the result of the two tensions. It balances the load λ, the resistance to the movement of LEM and BCR in opposite directions when their cells are in intimate contact (Fig. S7C). A similar resistance in the homologous tissue configuration in the zebrafish gastrula was modeled mechanically as a friction, and experimentally manipulated by altering mesoderm-ectoderm contact and tissue velocities (Smutny et al., 2017). The latter parameters vary naturally in the *Xenopus* gastrula during normal development.

The relative magnitudes of tensions and the angles between their directions change between time points and from plane to plane (Fig. 7E). Consistent with LEM attachment to the BCR in the rear region antagonizing LEM translocation (Fig. 6), the extent of rear contact parallels the load λ (Fig. 7F). For the two last time points, the load is lower than expected, perhaps due to directional migration of the LEM on the now slow-moving BCR. Overall, changes in BCR contact and velocity alter the load as predicted from the zebrafish friction model (Smutny et al., 2017). The magnitude of the BCR tension γ_r is constant as defined, but the angle between BCF and BCR changes dramatically. As γ_f increases, the BCR surface becomes more and more aligned with the BCF surface, until γ_f completely balances γ_r for a short time.

LEM tip cells are not a permanently differentiated cell type. They frequently change positions with cells that arrive from behind and move forward on the blastocoelic or the BCR-apposed LEM surface (Fig. 7I,J), rapidly integrating into a periodic pattern of ephrinB1 localization (Fig. S7C) and Ca^{2+} signaling (Hayashi et al., 2018).
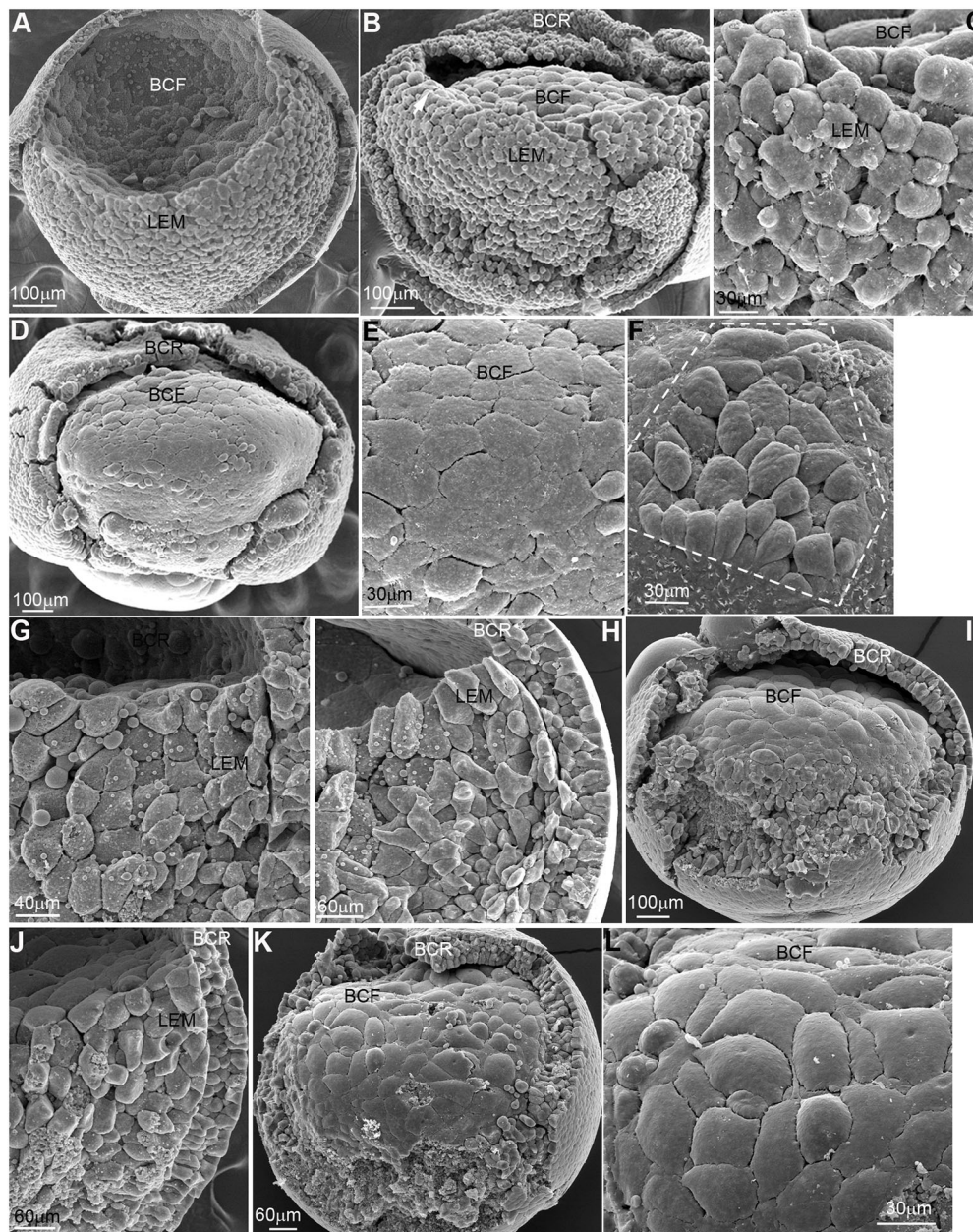
9

Fig. 9. LEM wedge shape depends on BCR interaction. (A) Mid-gastrula with the BCR removed after fixation, viewed from dorsal-animal side (n=12). (B) Gastrula fixed 1-2 min after removal of the BCR. LEM front collapsed (arrow) (n=5). (C) Higher magnification of B. (D) Embryo fixed 30 min after BCR removal (n=5). (E) Higher magnification of D. (F) In an embryo treated as in D, a piece of BCR was added after 30 min to the LEM surface for 5 min, then removed again (dashed outline) (n=5). (G) Sagittal fracture of the gastrula with PDGF-A knocked down in the BCR using a PDGF-A-MO (n=8; 2 experiments). (H,I) Phenotypes of gastrulae expressing dominant-negative PDGF-A in BCR (n=21; 4 experiments). (J-L) Embryos overexpressing PDGF-A in BCR (n=23; 5 experiments). (L) Higher magnification of LEM surface in K.

Tip cell-BCR contacts can be narrow, as in cadherin adhesions, or hundreds of nanometers wide (Fig. 7G,H; Fig. S7A,B). When BCR cusp surface and BCF are aligned, i.e. when γ_f is maximal, the force transmitted by a tip cell can be estimated. The BCR tissue surface tension is 0.2-0.6 mN/m (David et al., 2014). Assuming that this is the main component of γ_r, and with a tip cell width of 40 μm, a force of 8-24 nN/cell would have to be resisted to maintain attachment, which could be achieved by 150-450 cadherin bonds. The maximal possible link tension for cadherin-mediated adhesion is 200 nN/cell (Winklbauer, 2019), which is an order of magnitude higher than the value calculated for tip cells.

Shingle cell shear movement maintains the asymmetrical wedge shape of the LEM

The convex surface of the LEM is only intermittently and incompletely attached to the BCR, presumably to reduce the load λ. Given the liquid-like properties of gastrula tissues and

the presence of surface-minimizing tensions, the question arises of how a 'liquid' LEM wedge can be moved across a concave surface by being pulled at its tip (Fig. 8A). In principle, if a liquid rod with cylindrical minimal surface were attached to a fixed base and pulled by a force acting at the zenith (Fig. 8B), the surface on each side of the forming wedge would go from convex to concave, i.e. the curvature of the minimal surface from positive to negative, to permit volume conservation. Above a certain height, minimal surface conditions could no longer be reconciled with volume conservation, and capillary break up (Eggers, 1997; Montanero and Ponce-Torres, 2020) would occur.

In the absence of active cell movements, mean curvature would be equal for each side in a similarly pulled LEM as the Laplace pressure $p_L = \sigma (1/R_1 + 1/R_2)$ at both sides is the same at equilibrium, with R_1, R_2 principal radii of curvature on each surface (Fig. 8A) and σ the surface tension. To visualize problems arising from this condition, first the negative mean curvature of the BCF is applied to

both LEM sides (Fig. 8C). The sagittal curvature at the BCF is transferred to the BCR side, and the height of the wedge increased to conserve tissue volume (Fig. 8C, yellow). In addition, the now negative sagittal curvature on the BCR side must decrease further to compensate for the positive circumferential component of the mean curvature. This entails a further increase in height, virtual intersection of the two LEM surfaces (Fig. 8C, red) and, consequently, capillary break up of the LEM. Second, the positive curvature of the BCR-adjacent surface is similarly applied to both LEM sides (Fig. 8D, green). This leads to an angle between the BCF and BCR of 90° or less (see Fig. 9H), and the tip cells would retract the LEM in the vegetal direction.

Capillary break up or retraction were avoided if shingle cell movement maintained the asymmetric shape of the LEM wedge. In fact, the normal component of the force that drives cells obliquely towards the surface opposes the Laplace pressure generated by surface tension (Fig. 8E). At equilibrium, pressure p_f on the BCF surface and normal stress τ_{nf} generated by deep cells pulling at the BCF layer is balanced by p_r and normal stress τ_{nr} on the BCR-adjacent surface. With surface tensions σ_f and σ_r on BCF and BCR sides, respectively, principal radii of curvature $R_{f1} \approx \infty$ (as the inner LEM surface is almost straight in sagittal sections) and $R_{r1} = R_{r2} = R_r$ (as the LEM conforms to the spherical BCR), $-\sigma_f/R_{f2} + \tau_{nf} = 2\sigma_r/R_r - \tau_{nr}$. For $\sigma_r = \sigma_f$, and with $\tau_{nf} \approx \tau_{nr}$, $\sigma_f = 0.2$ mN/m (David et al., 2014) and radii $R_o = 530$ μm and $R_{i2} = 350$ μm, the normal stress would be $\tau_{nr} = 0.7$ N/m², and smaller for $\sigma_r < \sigma_f$. This corresponds closely to the condition that the normal stress completely balances the Laplace pressure, $2\sigma_r/R_r - \tau_{nr} = 0$, which gives a τ_{nr} of 0.75 N/m². With a cell cross-section of 1000 μm², and an angle between cell axis and surface of 45° (measured for 20 cells), the force generated per shingle cell is 1 nN, one order of magnitude lower than the force exerted by a tip cell.

Inside the LEM, the normal force of surface cells deforms the deep cells. At the BCF side, deep cells appear to pull obliquely on surface cells (Figs 1B, 7A-C), contributing to BCF layer tension and counteracting the pressure in the LEM (Fig. 8E). Ultimately, the forces generated by the shingled cells are thus transmitted to BCF layer and tip cells, and the torque generated keeps the LEM surface close to the BCR such that the asymmetrical LEM wedge is conforming to the BCR without adhering to it. In turn, proximity of the LEM to the BCR is necessary for this mechanism. When the BCR is experimentally removed, the tip cell rim collapses (Fig. 9A,B) and, within minutes (see Fig. 5A), the former BCR-adjacent side is indistinguishable from the BCF (Fig. 9C-E). Adding back a fragment of BCR restores loose cell packing (Fig. 9F). The BCR also controls the shingle arrangement of LEM cells (Nagel et al., 2004) and interfering with PDGF-A reveals how the loss of LEM cell orientation affects LEM shape and movement.

PDGF-A knockdown (Fig. 9G) or dominant-negative PDGF-A (Mercola et al., 1990; Nagel et al., 2004) (Fig. 9H,I) attenuate the advance of the LEM. Where it contacts the BCR, cell packing is loose (see also Fig. 5B) but a normal wedge does not form (Fig. 9G,H), and when the LEM detaches from the BCR, the surface becomes smooth (Fig. 9I). Overexpression of PDGF-A also disrupts cell orientation and causes the same two phenotypes (Fig. 9J-L), although lamellipodia still form (Nagel et al., 2004). Thus, the LEM in PDGF-inhibited embryos may begin to advance into available free space on the BCR (e.g. Fig. 9G,J), but instead of developing a normal wedge, LEM shapes consistent with capillary retraction form (Fig. 9H), or minimal surfaces that could be the result of either capillary retraction or break up (Fig. 9I,K,L). These data support the notion that active oriented cell-on-cell migration counters the disruptive effects of tissue surface

tension. In a feedback loop, the BCR controls cell motility in the LEM, which in turn ensures proximity of the LEM to the BCR without the need for direct attachment.

DISCUSSION

LEM translocation: a conserved movement in the primitive vertebrate gastrula

The movement of the LEM in the vertebrate gastrula appears to be a highly conserved process in taxa with a primitive mode of gastrulation. In the phylogenetically most basal vertebrate group, the lampreys, a LEM wedge is attached to a BCR cusp through tip cells, and a region of shingle cell arrangement behind the tip is detached from the BCR (de Selys-Longchamps, 1909). A similar structure is seen in sagittal gastrula sections of the frogs, *Rana* and *Bufo* (Komazaki, 1991; Johnson et al., 1993), and the newts, *Ambystoma* and *Pleurodeles* (Lundmark, 1986; Shi et al., 1989). For *Rana* and the newt *Triturus*, a shingle arrangement in anterior mesoderm with oriented protrusions of cells being attached to the cells in front of them has been described (Holtfreter, 1943).

These similarities suggest that, with its mechanism of movement, the composite structure of the LEM is conserved. The front and the blastocoelic side with BCF layer and with attached deep cells consist of large yolky cells, and are continuous with the endodermal vegetal cell mass. Cell-tracing and gene expression data indicate that these LEM cells are indeed derived from the vegetal mass and contribute to the endodermal gut (Bouwmeester et al., 1996; Jones et al., 1999; Papan et al., 2007; Zhang et al., 2016). At gastrulation, they provide the main components of the translocation machinery. The rear LEM region of small cells consists of blood-forming lateral plate mesoderm (Tracey et al., 1998), and it is carried along on the underside of the endodermal part of the LEM where it adds to the mechanical load, or migrates on the BCR surface, in particular at later stages. Thus, endoderm and mesoderm components are functionally integrated during translocation before they contribute to separate organ primordia after gastrulation.

LEM translocation as movement of a liquid tissue

The cohesion of gastrula tissues is based on flexible cell-cell adhesion that allows for cell rearrangement, and passive tissue behavior is characterized by the viscosity, surface tension and elasticity of a viscoelastic fluid (Steinberg, 1970; Gordon et al., 1972; Phillips et al., 1977; Davis, 1984; Foty et al., 1994; David et al., 2014; von Dassow et al., 2014). Surface tension naturally generates minimal surfaces, and active cell-on-cell migration is a mechanism with which to overcome this tendency and to generate the required shapes of tissues.

In the *Xenopus* gastrula, narrowing and lengthening of the chordamesoderm against its tendency to round up under interfacial tensions is driven by active, oriented cell intercalation (Ninomiya and Winklbauer, 2008). Tissue surface tension acts also on LEM translocation. To constrain its effects, the LEM could simply attach to the BCR and translocate by collective migration. The required velocity of 2.1 μm/min is within the range of isolated LEM cells (Wacker et al., 1998). However, when aggregated, the average velocity of the cells drops to 1 μm/min (Winklbauer and Nagel, 1991), and thus the LEM would be too slow to overcome fast epiboly of the BCR. LEM contact to the BCR is therefore effectively restricted to the tip where cells whose migratory potential is specifically increased by Ca^{2+} signaling (Hayashi et al., 2018) pull the LEM forward. This mode of movement, however, is subject to capillary retraction or break up (Eggers, 1997; Montanero and Ponce-Torres, 2020).

We propose that adverse effects of tissue surface tension are prevented by combining tip pulling with oriented cell-on-cell migration behind the tip. The tip moving forward tends to separate the barely attached LEM from the curved BCR (Fig. 10A,B), but before the free LEM surface caves in, its cells crawl obliquely towards the BCR to maintain its curvature (Fig. 10B,C). In this process, cell motility is controlled by signals from the BCR, and at the same time the LEM is kept close to the BCR without permanently attaching to it. The LEM can hover over the curved BCR substratum without its advance being attenuated by epiboly, while still receiving all BCR signals required.

LEM-BCR interactions

BCR signaling to the LEM is required for LEM detachment from the BCR, for lamellipodia formation and for orienting LEM cells to attain a shingle arrangement. Prechordal mesoderm-BCR separation is based on Eph receptor-ephrin signaling during short phases of attachment, which results in cell repulsion and reduced mesoderm cohesion (Rohani et al., 2011, 2014). This mechanism has yet to be demonstrated for the LEM, but when the BCR is experimentally removed, LEM cells form a compact surface within minutes – a sign of regained cohesion. As episodes of BCR-LEM separation in the embryo last longer than cohesion needs to recover, mechanisms beyond direct cell contact must control detachment. Signaling across a detachment gap could be mediated by filopodia or exosomes (Gong et al., 2016; Takasugi et al., 2017; Valenzuela and Perez, 2020), which would require proximity to the BCR, but not intimate contact.

Proximity of LEM and BCR is also necessary to sustain lamellipodia, as BCR-derived PDGF-A diminishes their contact inhibition in the LEM (Nagel and Winklbauer, 2018). sf-PDGF-A diffuses rapidly from the BCR into the LEM (Damm, 2014) and should thus be present in the cleft between BCR and LEM to continuously support lamellipodia. The occasional attachment of lamellipodia to the BCR depends on FN (Nakatsuji, 1975; Winklbauer and Selchow, 1992; Winklbauer and Keller, 1996). Switching lamellipodia attachment from the LEM surface to the BCR while maintaining shingle arrangement and migration could reduce the load during temporary LEM rear region adhesion to the BCR and drive the movement when epiboly has slowed down later in gastrulation.

Most importantly, the BCR is required for the orientation of LEM cell lamellipodia via the BCR extracellular matrix (Nakatsuji and Johnson, 1983; Winklbauer and Nagel, 1991; Winklbauer et al., 1992). The matrix directs the accumulation of PDGF receptor to the animal side of cells, and matrix-bound lfPDGF-A favors the survival of PDGF receptor-enriched lamellipodia, thus biasing protrusive activity (Nagel and Winklbauer, 2018). Once established, cell orientation could be maintained for some time during detachment. It could also spread from the tip cells in contact with the BCR to the cells behind by mechanical (Sonavane et al., 2017) or Wnt signaling (Li and Wang, 2018).

Vertical shearing, a form of morphogenetic cell rearrangement

When obliquely oriented cell-on-cell migration occurs all along the length the LEM, and each cell moves outward in relation to the cell in front of it, this will tilt the surface layer by an out-of-plane shear movement (Fig. 10D). The process resembles epithelial invagination by vertical telescoping (Li et al., 2020). Instead of epithelial bending by apical constriction, telescoping involves vertical shear movement of cells relative to each other, organized around a center. Movements add up such that more-peripheral cells move proportionally more and a pit forms in the center (Fig. 10E). The cells extend oriented protrusions across each other's apical surfaces (Li et al., 2020) (Fig. 10E), strongly resembling cells on the LEM surface. These shared features define a type of cell rearrangement which could be termed 'vertical shearing'. Vertical telescoping of epithelia and out-of-plane shearing of cell mass surfaces would be examples of this morphogenetic mechanism (Fig. 10D,E).

As characteristic for intercalation movements, the staggered displacement of individual cells adds up such that small changes in relative cell positions lead to major tissue shape changes. A given cell in an array is moved passively as it is attached to the cell in front of it but, in addition, it moves on this cell by using its own activity (Fig. 10D). In the case of the LEM, to close a typical BCR-LEM cleft half a cell diameter wide and five cells long by vertical shearing, each cell must move 1/8th of a cell diameter, about 4 µm, during an attachment-detachment cycle of tens of minutes. This implies displacement rates that are barely noticeable and do not lead
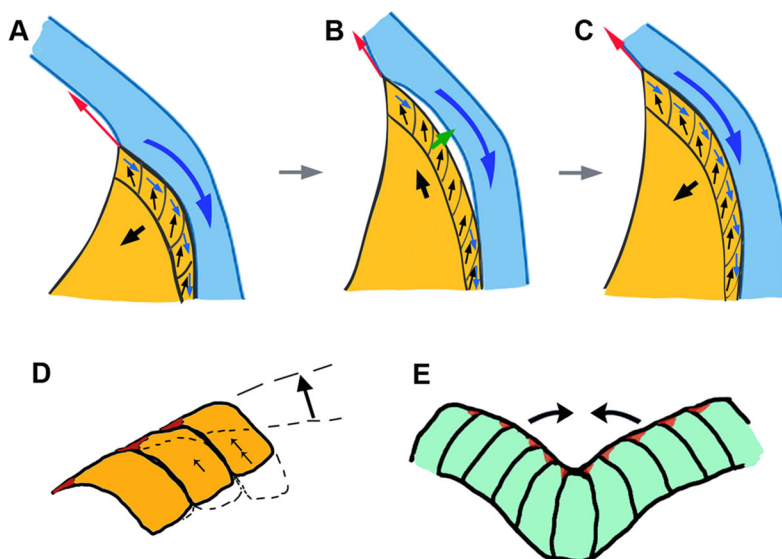

Fig. 10. LEM translocation and vertical shearing. (A-C) A liquid-like LEM wedge (orange) pulled by tip cells (red arrow) against the epibolic flow of the BCR (blue, large blue arrow). When closely attached to the BCR, LEM cells at the interface are pulled vegetally (small blue arrows) by the BCR (A,C). Pulling at its tip and rear end tends to separate the LEM from the curved BCR (large black arrows in A,C), generating a gap (B). This allows the LEM to move forward (large black arrow), but LEM surface cells moving obliquely towards the BCR (small black arrows) prevent full detachment and collapse of the LEM, and move its surface back to the BCR (large green arrow), until the cycle is repeated. (D) Shear movement of the LEM surface cells – vertical shearing – tilts the LEM surface (large black arrow). Active movement of a cell on the back of a cell ahead, and passive displacement due to active movements of all cells ahead, add up from front to back (small arrows). Dashed outlines indicate the original positions of cells; red pointed ends indicate lamellipodia. (E) When oriented around a center, the same mechanism of vertical shearing leads to epithelial invagination by vertical telescoping.

to large-scale cell rearrangement. Nevertheless, the summed-up effect ensures proximity of the LEM to the curved BCR.

MATERIALS AND METHODS

Embryos, micromanipulations and injections
Xenopus laevis were bred in-house and kept according to University of Toronto Animal Use Protocol 20011765. Embryos from *in vitro* fertilized eggs were de-jellied with 2% cysteine in 1/10 Modified Barth's Solution [MBS; 88 mM NaCl, 1 mM KCl, 2.4 mM NaHCO$_3$, 0.82 mM MgSO$_4$, 0.33 mM Ca(NO$_3$)$_2$, 0.41 mM CaCl$_2$, 10 mM Hepes (+NaOH), 1% streptomycin, 1% penicillin (pH 7.4) (pH 8.0)]. Embryos were injected at the four-cell stage in both dorsal blastomeres using a Nanoinject II (Drummond Scientific Company) in 4% Ficoll, and cultured at 15°C in 1/10 MBS until gastrula stages.

Preparation of substrata
Tissue culture dishes (35 mm) with a polymer coverslip bottom from Ibidi were coated with bovine plasma FN (Sigma) at 200 ng/ml for 1 h or C-cadherin-Fc 200 ng/ml for 1 h (Zhong et al., 1999) and saturated with 1 mg/ml of bovine serum albumin (BSA) for 30 min or were uncoated and saturated with 1 mg/ml BSA. For single cell analysis, the explants were incubated for 20 min in Dissociation Buffer [88 mM NaCl, 1 mM KCl, 2.4 mM NaHCO$_3$, 10 mM Hepes (+NaOH), 1% streptomycin, 1% penicillin (pH 7.4)].

Microsurgery
Embryos were staged according to Nieuwkoop and Faber (1967). At gastrula stage 10.5, the vitelline membrane was removed with forceps. Microsurgery was performed in MBS at room temperature under a MZ16F (Leica) stereomicroscope. The LEM was excised and placed on prepared substrata for imaging. Single cells were obtained by dissociating mesendoderm aggregates in Dissociation Buffer [88 mM NaCl, 1 mM KCl, 2.4 mM NaHCO$_3$, 10 mM Hepes (+NaOH), 1% streptomycin, and 1% penicillin (pH 7.4)]. Operation techniques have been described previously (Winklbauer, 1990; Winklbauer and Schürfeld, 1999).

Constructs, mRNA synthesis and injection
CS2+mbGFP from R. Harland (University of California, Berkeley, USA) and mbRFP (a gift from A. Bruce, University of Toronto, Canada) were linearized with NotI and transcribed with SP6 polymerase. A kinase-dead mutant K281A of xPak1 (KD-Pak1) (Poitras et al., 2003; Bisson et al., 2003) was linearized with XbaI and transcribed with T7 polymerase. Embryos were injected at the four-cell stage marginally into the dorsal two blastomeres. Plasmid pGHE2 containing the long form and the short form of *Xenopus* PDGFA (lf-PDGFA, sf-PDGFA) (Mercola et al., 1988), were linearized with *Nhe*I and transcribed with T7 polymerase. A C-terminally truncated form of lf-PDGF-A, sf-PDGF-A, lacking the matrix-binding motif (amino acid residues 198-227) in pCS2 was used for *in vitro* transcription with SP6 polymerase after linearization with *Xho*I. Embryos were injected at the four-cell stage marginally into the dorsal two blastomeres. Plasmid pGHE2 harboring a processing defective mutant of mouse PDGF-A acting as a dominant-negative in *Xenopus* (Mercola et al., 1990) was linearized with NheI and transcribed with T7 polymerase. mRNA amounts injected per blastomere were as follows: mbGFP, 150 pg; mbRFP, 100 pg; KD-Pak1, 300 pg; Sf-PDGF-A, 200 pg; Lf-PDGF-A, 200 pg; and DN-PDGF-A, 200 pg. Morpholino antisense oligonucleotides were as follows: xFN1, 5′ CGCTCTGGAGACTATAAAAGCCAAT 3′ (18 ng; Davidson et al., 2006); xFN2, 5′ CGCATTTTTCAAACGCTCTGAAGAC 3′ (18 ng); xPDGF, 5′ AGAATCCAAGCCCAGATCCTCATTG 3′ (20 ng; Nagel et al., 2004); xC-cadh, 5′ CCACCGTCCCGAACAGAAGCCTCAT 3′ (20 ng; Ninomiya et al., 2012); and xR-cadh, 5′ CAGTCATACTGCTCC-CGGTCTCGGT 3′ (20 ng; Rungger-Brandle et al., 2010).

Histology
F-actin was stained in specimens fixed in 4% paraformaldehyde (20 min, 0.01% Triton-X-100 added after 5 min) with Alexa Fluor 488 phalloidin, Alexa Fluor 647 (Thermo Fisher Scientific) or rhodamine phalloidin (Invitrogen) at 1:100 in PBS/BSA for 20 min. Rabbit antiserum against *Xenopus laevis* plasma FN (Winklbauer, 1998) (1:1000), mouse monoclonal antibody 8C8 against *Xenopus laevis* integrinβ1 (DSHB, P. Hausen and V. Gawantka, Max-Planck-Institute for Developmental Biology, Tübingen, Germany) (1:6), monoclonal antibody 6B6 anti-Xenopus C-cadherin (Hybridoma Bank) (Choi et al., 1990) and polyclonal rabbit antibody against ephrin B1 (A-20; sc-1011, Santa Cruz Biotechnology; 1:200) were used. Secondary antibodies were Cy3-goat-anti-rabbit IgG, FITC-goat-anti-rabbit IgG, and Cy3-goat-anti-mouse IgG (Jackson Immuno Research Labs). Staining intensity was measured using the Leica Application Suite X software. For image collection, a SP8-nonresonant confocal microscope (Leica) with 40× immersion oil objective and a Zeiss Axiovert 200M microscope (PlanNeofluar 20× and 40× oil objectives) with Leica Application SuiteX software or AxioVision LE64 software were used. Nile Blue staining of live embryos was performed according to Kirschner and Hara (1980).

Histological sections and TEM
Kinase-dead Pak1-expressing LEM explants were cultured for 2 h and then fixed overnight at 4°C in 3% GA and 2% PFA in 1× PBS (pH 7.0). Explants were then rinsed using 1× PBS, bisected and fixed overnight at 4°C in 1× PBS containing 1% OsO$_4$. Explants were then rinsed again using PBS, dehydrated in a graded series of ethanol, embedded in 100% Spurr's resin and cured at 65°C for 24 h. Ultrathin (90-100 nm) sections were obtained using a Leica EM UC6 microtome and stained with 3% uranyl acetate in methanol for 1 h and Reynold's lead citrate for 10 min. TEM images were taken with the Hitachi HT7700 microscope. The position and extend of the LEM was determined according to Damm and Winklbauer (2011).

Scanning electron microscopy
Embryos were fixed in 2.5% glutaraldehyde/0.1 M sodium cacodylate overnight at 4°C, post-fixed in osmium tetraoxide and dehydrated in an ethanol/0.1 M cacodylate and ethanol/hexamethyl-disilizane series. Specimens were dried overnight, mounted on SEM stubs using conductive carbon tape (Structure Probe), and sputter coated with gold-palladium (60%/40%) for 50 s. Specimens were imaged with a Hitachi S-2500 scanning electron microscope.

Time-lapse X-ray phase-contrast micro-tomography (TXPCµT)
TXPCµT has been previously described (Moosmann et al., 2013, 2014). In short, the time-lapse series used was from microtomography performed at beamline station 2-BM-B of Advanced Photon Source (monochromatization of $\Delta E/E=10^{-2}$, flux density of $\sim10^{12}$ photons per second per mm^2, hutch temperature $\sim25°C$). The set-up was optimized for low dose deposition (15 ms exposure per projection, $n=1200$ projections, 18 s to record one tomogram with continuous rotation of sample) at sufficient image contrast, avoiding blurring effects due to cell motion and source size (3.4 µm horizontal image blurring at $z=62$ cm, horizontal coherence length of ~4.2 µm). A filtered back-projection algorithm was applied to compute the 3D distribution of electron density. The waiting time between tomographic recordings was 10 min. An X-ray dose of about 300 Gy was applied throughout each tomographic recording due to residual absorption, which does not generate any useable image contrast, and it has been confirmed by Moosmann et al. (2013) that, in spite of this relatively large dose, the major processes of gastrulation proceed in a wild-type fashion. This 4D imaging modality seems to be less applicable for long-term monitoring of more differentiated stages of development where locally applied dose may inhibit tissue dynamics and impair the formation of functional units.

DEVELOPMENT

Supplementary information
Supplementary information available online at
https://dev.biologists.org/lookup/doi/10.1242/dev.198960.supplemental

Peer review history
The peer review history is available online at
https://dev.biologists.org/lookup/doi/10.1242/dev.198960.reviewer-comments.pdf

References
Ataliotis, P., Symes, K., Chou, M. M., Ho, L. and Mercola, M. (1995). PDGF signaling is required for gastrulation of *Xenopus laevis*. *Development* **121**, 3099-3110.
Bisson, N., Islam, N., Poitras, L., Jean, S., Bresnick, A. and Moss, T. (2003). The catalytic domain of xPAK1 is sufficient to induce myosin II dependent in vivo cell fragmentation independently of other apoptotic events. *Dev. Biol.* **263**, 264-281. doi:10.1016/j.ydbio.2003.07.002
Bouwmeester, T., Kim, S.-H., Sasai, Y., Lu, B. and De Robertis, E. M. (1996). Cerberus is a head-inducing secreted factor expressed in the anterior endoderm of Spemann's organizer. *Nature (Lond.)* **382**, 595-601. doi:10.1038/382595a0
Choi, Y. S., Sehgal, R., McCrea, P. and Gumbiner, B. (1990). A cadherin-like protein in eggs and cleaving embryos of Xenopus laevis is expressed in oocytes in response to progesterone. *J. Cell Biol.* **110**, 1575-1582. doi:10.1083/jcb.110.5.1575
Damm, E. W. (2014). PDGF-A Signalling Regulates Radially Oriented Movements of Mesoderm Cells During Gastrulation in *Xenopus*. *PhD Thesis*, University of Toronto, Canada.
Damm, E. W. and Winklbauer, R. (2011). PDGF-A controls mesoderm cell orientation and radial intercalation during *Xenopus* gastrulation. *Development* **138**, 565-575. doi:10.1242/dev.056903
David, R., Luu, O., Damm, E. W., Wen, J. W. H., Nagel, M. and Winklbauer, R. (2014). Tissue cohesion and the mechanics of cell rearrangement. *Development* **141**, 3672-3682. doi:10.1242/dev.104315
Davidson, L. A., Marsden, M., Keller, R. and Desimone, D. W. (2006). Integrin $\alpha5\beta1$ and fibronectin regulate polarized cell protrusions required for *Xenopus* convergence and extension. *Curr. Biol.* **16**, 833-844. doi:10.1016/j.cub.2006.03.038
Davis, G. S. (1984). Migration-directing liquid properties of embryonic amphibian tissues. *Am. Zool.* **24**, 649-655. doi:10.1093/icb/24.3.649
de Selys-Longchamps, M. (1909). Gastrulation et formation des feuillets chez *Petromyzon Planeri*. *Arch. Biol.* **25**, 1-75.
Eggers, J. (1997). Non-linear dynamics and break-up of free-surface flows. *Rev. Mod. Phys.* **69**, 865-930. doi:10.1103/RevModPhys.69.865
Foty, R. A., Forgacs, G., Pfleger, C. M. and Steinberg, M. S. (1994). Liquid properties of embryonic tissues: measurement of interfacial tensions. *Phys. Rev. Lett.* **72**, 2298-2301. doi:10.1103/PhysRevLett.72.2298
Gong, J., Körner, R., Gaitanos, L. and Klein, R. (2016). Exosomes mediate cell contact-independent ephrin-Eph signaling during axon guidance. *J. Cell Biol.* **214**, 35-44. doi:10.1083/jcb.201601085
Gordon, R., Goel, N. S., Steinberg, M. S. and Wiseman, L. L. (1972). A rheological mechanism sufficient to explain the kinetics of cell sorting. *J. theor. Biol.* **37**, 43-73. doi:10.1016/0022-5193(72)90114-2
Hayashi, K., Yamamoto, T. S. and Ueno, N. (2018). Intracellular calcium signal at the leading edge regulates mesodermal sheet migration during *Xenopus* gastrulation. *Sci. Rep.* **8**, 2433. doi:10.1038/s41598-018-20747-w
Holtfreter, J. (1943). Properties and functions of the surface coat in amphibian embryos. *J. Exp. Zool.* **93**, 251-323. doi:10.1002/jez.1400930205
Ibrahim, H. and Winklbauer, R. (2001). Mechanisms of mesendoderm internalization in the *Xenopus* gastrula: lessons from the ventral side. *Dev. Biol.* **240**, 108-122. doi:10.1006/dbio.2001.0459
Johnson, K. E., Darribère, T. and Boucaut, J.-C. (1993). Mesodermal cell adhesion to fibronectin-rich fibrillar extracellular matrix is required for normal *Rana pipiens* gastrulation. *J. Exp. Zool.* **265**, 40-53. doi:10.1002/jez.1402650107

Jones, C. M., Broadbent, J., Thomas, P. Q., Smith, J. C. and Beddington, R. S. P. (1999). An anterior signalling centre in *Xenopus* revealed by the homeobox gene Xhex. *Curr. Biol.* **9**, 946-954. doi:10.1016/S0960-9822(99)80421-7
Keller, R. E. (1976). Vital dye mapping of the gastrula and neurula of *Xenopus laevis*. II. Prospective areas and morphogenetic movements of the deep layer. *Dev. Biol.* **51**, 118-137. doi:10.1016/0012-1606(76)90127-5
Kirschner, M. W. and Hara, K. (1980). A new method for local vital staining of amphibian embryos using Ficoll and "crystals" of Nile Red. *Mikroskopie* **36**, 12-15.
Komazaki, S. (1991). Changes in intercellular contacts, motility, and adhesiveness of the presumptive mesodermal cells of *Bufo vulgaris* embryos before and during gastrulation. *J. Exp. Zool.* **258**, 327-335. doi:10.1002/jez.1402580308
Li, D. and Wang, Y.-l. (2018). Coordination of cell migration mediated by site-dependent cell-cell contact. *Proc. Natl. Acad. Sci. USA* **115**, 10678-10683. doi:10.1073/pnas.1807543115
Li, J., Economou, A. D., Vacca, B. and Green, J. B. A. (2020). Epithelial invagination by a vertical telescoping cell movement in mammalian salivary glands and teeth. *Nat. Commun.* **11**, 2366. doi:10.1038/s41467-020-16247-z
Lundmark, C. (1986). Role of bilateral zones of ingresssing superficial cells during gastrulation of *Ambystoma mexicanum*. *J. Embryol. Exp. Morph.* **97**, 47-62.
Luu, O., David, R., Ninomiya, H. and Winklbauer, R. (2011). Large-scale mechanical properties of *Xenopus* embryonic epithelium. *Proc. Natl. Acad. Sci. USA* **108**, 4000-4005. doi:10.1073/pnas.1010331108
Luu, O., Damm, E. W., Parent, S. E., Barua, D., Smith, T. H. L., Wen, J. W. H., Lepage, S. E., Nagel, M., Ibrahim-Gawel, H., Huang, Y. et al. (2015). PAPC mediates self/non-self-distinction during Snail1-dependent tissue separation. *J. Cell Biol.* **208**, 839-856. doi:10.1083/jcb.201409026
Mercola, M., Melton, D. A. and Stiles, C. D. (1988). Platelet-derived growth factor A chain is maternally encoded in *Xenopus* embryos. *Science* **241**, 1223-1225. doi:10.1126/science.3413486
Mercola, M., Deininger, P. L., Shamah, S. M., Porter, J., Wang, C. Y. and Stiles, C. D. (1990). Dominant-negative mutants of a platelet-derived growth factor gene. *Genes Dev.* **4**, 2333-2341. doi:10.1101/gad.4.12b.2333
Montanero, J. M. and Ponce-Torres, A. (2020). Review on the dynamics of isothermal liquid bridges. *Appl. Mechan. Reviews* **72**, 101803. doi:10.1115/1.4044467
Moosmann, J., Ershov, A., Altapova, V., Baumbach, T., Prasad, M. S., LaBonne, C., Xiao, X., Kashef, J. and Hofmann, R. (2013). X-ray phase-contrast in vivo microtomography probes new aspects of *Xenopus* gastrulation. *Nature* **497**, 374-377. doi:10.1038/nature12116
Moosmann, J., Ershov, A., Weinhardt, V., Baumbach, T., Prasad, M. S., LaBonne, C., Xiao, X., Kashef, J. and Hofmann, R. (2014). Time-lapse X-ray phase-contrast microtomography for in vivo imaging and analysis of morphogenesis. *Nat. Protoc.* **9**, 294-304. doi:10.1038/nprot.2014.033
Nagel, M. and Winklbauer, R. (1999). Establishment of substratum polarity in the blastocoel roof of the *Xenopus* embryo. *Development* **126**, 1975-1984.
Nagel, M. and Winklbauer, R. (2018). PDGF-A suppresses contact inhibition during directional collective cell migration. *Development* **145**, 1-15. pii: dev162651. doi:10.1242/dev.162651
Nagel, M., Tahinci, E., Symes, K. and Winklbauer, R. (2004). Guidance of mesoderm cell migration in the *Xenopus* gastrula requires PDGF signaling. *Development* **131**, 2727-2736. doi:10.1242/dev.01141
Nakatsuji, N. (1975). Studies on the gastrulation of amphibian embryos: cell movement during gastrulation in *Xenopus laevis* embryos. *Wilhelm Roux' Archiv* **178**, 1-14. doi:10.1007/BF00848358
Nakatsuji, N. and Johnson, K. E. (1983). Conditioning of a culture substratum by the ectodermal layer promotes attachment and oriented locomotion by amphibian gastrula mesodermal cells. *J. Cell Sci.* **59**, 43-60.
Nakatsuji, N., Smolira, M. A. and Wylie, C. C. (1985). Fibronectin visualized by scanning electron microscopy immunocytochemistry on the substratum for cell migration in *Xenopus laevis* gastrulae. *Dev. Biol.* **107**, 264-268. doi:10.1016/0012-1606(85)90395-1
Nieuwkoop, P. D. and Faber, J. (1967). *Normal Table of Xenopus laevis (Daudin)*. Amsterdam: North-Holland Publishing Company.
Nieuwkoop, P. D. and Florschutz, P. A. (1950). Quelques caracteres speciaux de la gastrulation et de la neurulation de l'oeuf de *Xenopus laevis*, Daud. Et de quelques autres Anoures. 1ere partie. Etude descriptive. *Arch. Biol.* **61**, 113-150.
Ninomiya, H. and Winklbauer, R. (2008). Epithelial coating controls mesenchymal shape change through tissue-positioning effects and reduction of surface-minimizing tension. *Nat. Cell Biol.* **10**, 61-69. doi:10.1038/ncb1669
Ninomiya, H., David, R., Damm, E. W., Fagotto, F., Niessen, C. M. and Winklbauer, R. (2012). Cadherin-dependent differential cell adhesion in *Xenopus* causes cell sorting in vitro but not in the embryo. *J. Cell Sci.* **125**, 1877-1883. doi:10.1242/jcs.095315
Papan, C., Boulat, B., Velan, S. S., Fraser, S. E. and Jacobs, R. E. (2007). Formation of the dorsal marginal zone in *Xenopus laevis* analyzed by time-lapse microscopic magnetic resonance imaging. *Dev. Biol.* **305**, 161-171. doi:10.1016/j.ydbio.2007.02.005
Phillips, H. M., Steinberg, M. S. and Lipton, B. H. (1977). Embryonic tissues as elasticoviscous liquids: II. Direct evidence for cell slippage in centrifuged aggregates. *Dev. Biol.* **59**, 124-134. doi:10.1016/0012-1606(77)90247-0

DEVELOPMENT

14

Poitras, L., Jean, S., Islam, N. and Moss, T. (2003). PAK interacts with NCK and MLK2 to regulate the activation of jun N-terminal kinase. *FEBS Lett.* **543**, 129-135. doi:10.1016/S0014-5793(03)00424-1

Rohani, N., Canty, L., Luu, O., Fagotto, F. and Winklbauer, R. (2011). EphrinB/EphB signaling controls embryonic germ layer separation by contact-induced cell detachment. *PLoS Biol.* **9**, e1000597. doi:10.1371/journal.pbio.1000597

Rohani, N., Winklbauer, R. and Fagotto, F. (2014). Ephrin-Eph signaling in embryonic tissue separation. *Cell Adh. Migr.* **8**, 308-326. doi:10.4161/19336918.2014.970028

Rungger-Brändle, E., Ripperger, J. A., Steiner, K., Conti, A., Stieger, A. and Rungger, D. (2010). Retinal patterning by Pax6–dependent cell adhesion molecules. *Dev. Neurobiol.* **70**, 764-780. doi:10.1002/dneu.20816

Shi, D.-L., Darribere, T., Johnson, K. E. and Boucaut, J.-C. (1989). Initiation of mesodermal cell migration and spreading relative to gastrulation in the urodele amphibian *Pleurodeles waltl*. *Development* **105**, 351-363.

Smutny, M., Ákos, Z., Grigolon, S., Shamipour, S., Ruprecht, V., Čapek, D., Behrndt, M., Papusheva, E., Tada, M., Hof, B. et al. (2017). Friction forces position the neural anlage. *Nat. Cell Biol.* **19**, 306-317. doi:10.1038/ncb3492

Sonavane, P. R., Wang, C., Dzamba, B., Weber, G. F., Periasamy, A. and DeSimone, D. W. (2017). Mechanical and signaling roles for keratin intermediate filaments in the assembly and morphogenesis of *Xenopus* mesendoderm tissue at gastrulation. *Development* **144**, 4363-4376. doi:10.1242/dev.155200

Steinberg, M. S. (1970). Does differential adhesion govern self-assembly processes in histogenesis? Equilibrium configurations and the emergence of a hierarchy among populations of embryonic cells. *J. Exp. Zool.* **173**, 395-434. doi:10.1002/jez.1401730406

Takasugi, M., Okada, R., Takahashi, A., Chen, D. V., Watanabe, S. and Hara, E. (2017). Small extracellular vesicles secreted from senescent cells promote cancer cell proliferation through EphA2. *Nat. Commun.* **8**, 15728. doi:10.1038/ncomms15728

Tashiro, K., Tooi, O., Nakamura, H., Koga, C., Ito, Y., Hikasa, H. and Shiokawa, K. (1995). Cloning and expression studies of cDNA for a novel *Xenopus* cadherin (XmN-cadherin), expressed maternally and later neural-specifically in embryogenesis. *Mech. Dev.* **54**, 161-171. doi:10.1016/0925-4773(95)00469-6

Tracey, W. D., Jr, Pepling, M. E., Horb, M. E., Thomsen, G. H. and Gergen, J. P. (1998). A *Xenopus* homologue of aml-1 reveals unexpected patterning mechanisms leading to the formation of embryonic blood. *Development* **125**, 1371-1380.

Valenzuela, J. I. and Perez, F. (2020). Localized intercellular transfer of ephrin-As by trans-endocytosis enables long-term signaling. *Dev. Cell* **52**, 104-117.e5. doi:10.1016/j.devcel.2019.11.013

von Dassow, M., Miller, C. J. and Davidson, L. A. (2014). Biomechanics and the thermotolerance of development. *PLoS ONE* **9**, e95670. doi:10.1371/journal.pone.0095670

Wacker, S., Brodbeck, A., Lemaire, P., Niehrs, C. and Winklbauer, R. (1998). Patterns and control of cell motility in the *Xenopus* gastrula. *Development* **125**, 1931-1942.

Wen, J. W. H. and Winklbauer, R. (2017). Ingression-type cell migration drives vegetal endoderm internalisation in the *Xenopus* gastrula. *eLife* **6**, e27190. doi:10.7554/eLife.27190

Winklbauer, R. (1990). Mesodermal cell migration during *Xenopus* gastrulation. *Dev. Biol.* **142**, 155-168. doi:10.1016/0012-1606(90)90159-G

Winklbauer, R. (1998). Conditions for fibronectin fibril formation in the early *Xenopus* embryo. *Dev. Dyn.* **212**, 335-345. doi:10.1002/(SICI)1097-0177(199807)212:3<335::AID-AJA1>3.0.CO;2-I

Winklbauer, R. (2019). Dynamic cell-cell adhesion mediated by pericellular matrix interaction - a hypothesis. *J. Cell Sci.* **132**, 1-10. jcs231597. doi:10.1242/jcs.231597

Winklbauer, R. (2020). Mesoderm and endoderm internalization in the Xenopus gastrula. *Curr. Top. Dev. Biol.* **136**, 243-270. doi:10.1016/bs.ctdb.2019.09.002

Winklbauer, R. and Keller, R. E. (1996). Fibronectin, mesoderm migration, and gastrulation in *Xenopus*. *Dev. Biol.* **177**, 413-426. doi:10.1006/dbio.1996.0174

Winklbauer, R. and Nagel, M. (1991). Directional mesoderm cell migration in the *Xenopus* gastrula. *Dev. Biol.* **148**, 573-589. doi:10.1016/0012-1606(91)90275-8

Winklbauer, R. and Parent, S. E. (2016). Forces driving cell sorting in the amphibian embryo. *Mech. Dev.* **144**, 81-91. doi:10.1016/j.mod.2016.09.003

Winklbauer, R. and Schürfeld, M. (1999). Vegetal rotation, a new gastrulation movement involved in the internalization of the mesoderm and endoderm in *Xenopus*. *Development* **126**, 3703-3713.

Winklbauer, R. and Selchow, A. (1992). Motile behavior and protrusive activity of migratory mesoderm cells from the *Xenopus* gastrula. *Dev. Biol.* **150**, 335-351. doi:10.1016/0012-1606(92)90246-D

Winklbauer, R., Selchow, A., Nagel, M. and Angres, B. (1992). Cell interaction and its role in mesoderm cell migration during *Xenopus gastrulation*. *Dev. Dyn.* **195**, 290-302. doi:10.1002/aja.1001950407

Zhang, Z., Rankin, S. A. and Zorn, A. M. (2016). Syndecan4 coordinates Wnt/JNK and BMP signaling to regulate foregut progenitor development. *Dev. Biol.* **416**, 187-199. doi:10.1016/j.ydbio.2016.05.025

Zhong, Y., Brieher, W. M. and Gumbiner, B. M. (1999). Analysis of C-cadherin regulation during tissue morphogenesis with an activating antibody. *J. Cell Biol.* **144**, 351-359. doi:10.1083/jcb.144.2.351

Zimmerman, S. P., Asokan, S. B., Kuhlman, B. and Bear, J. E. (2017). Cells lay their own tracks – optogenetic Cdc42 activation stimulates fibronectin deposition supporting directed migration. *J. Cell Sci.* **130**, 2971-2983. doi:10.1242/jcs.205948

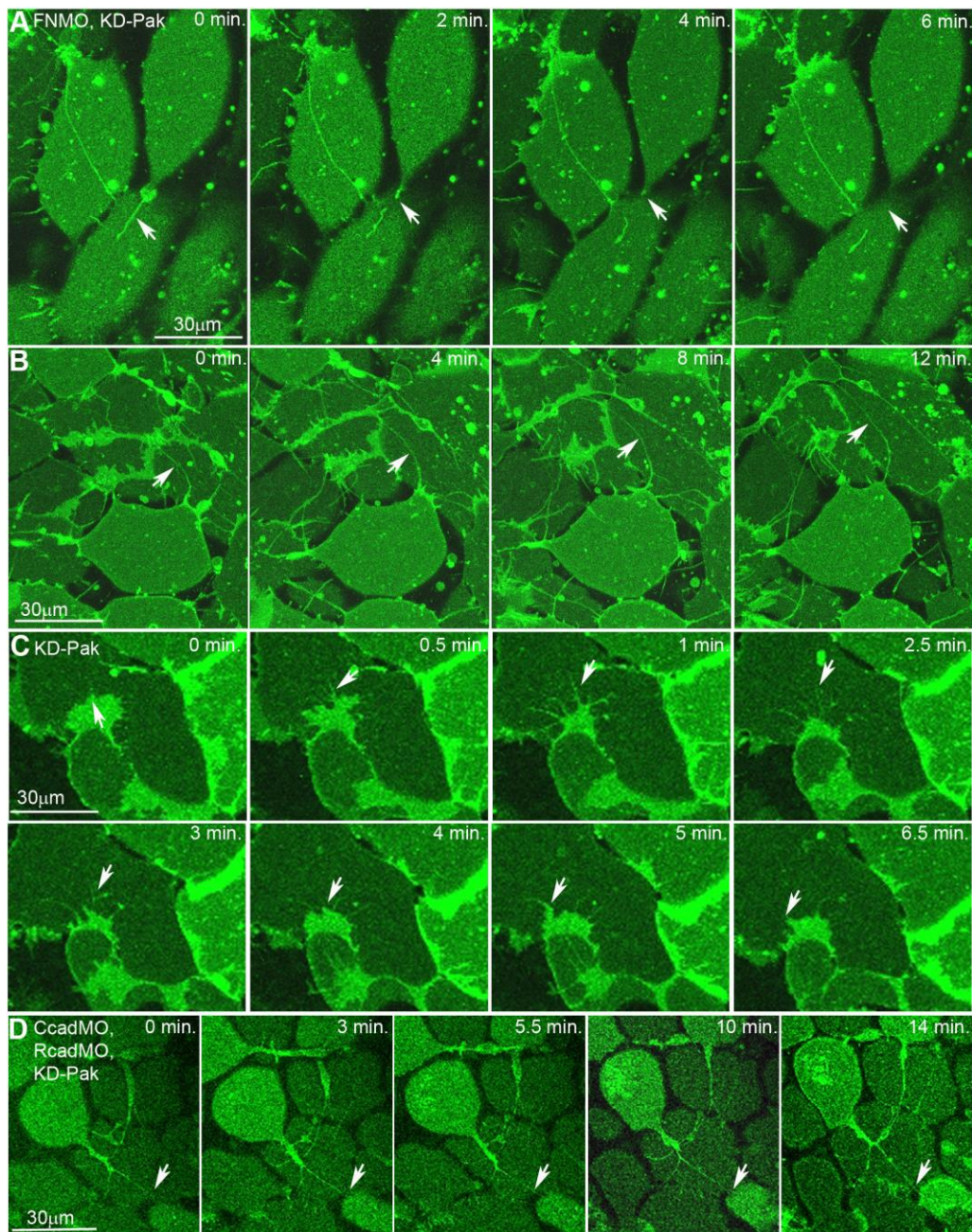**Supplementary Material** - **Supplementary Figures**

Figure S1. Fibronectin and cadherin requirements for lamellipodia retraction. Time lapse recordings of kinase-dead Pak1/membrane-GFP expressing LEM explants with (A,B) (n=7; 2 experiments) or without FN-MO injection (C) (n=5; 2 experiments), or with coinjection of C-cad-MO and R-cad-MO (D) (n=10; 2 experiments). Arrows, retracting or breaking retraction fibers.
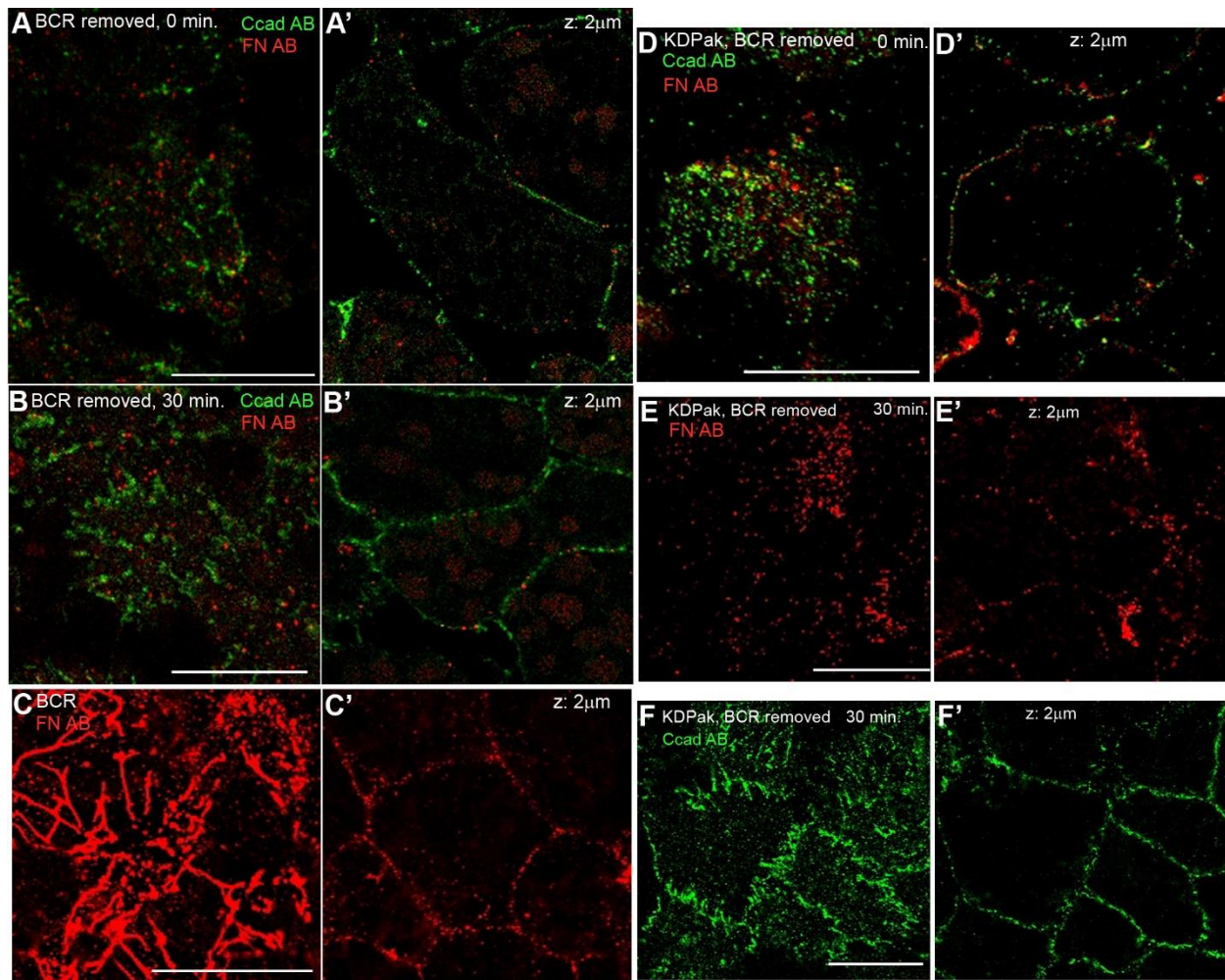
Figure S2. csFN and C-cadherin on the surface of cells. (A,D) BCR-facing side of untreated (n=28; 2 experiments) or kinase-dead Pak1 expressing LEM (n=17) stained immediately after BCR removal for FN (red) and C-cadherin (green), viewed at surface (A,D) and deep in tissue (A',D'). (B,B') Same as (A,A') but fixed and stained 30 minutes after removal of BCR (n=14). (E-F') same as (B,B') but with kinase-dead Pak1 expressing LEM stained for FN (E,E') (n=14) and C-cadherin (F,F') (n=15). (C,C') FN staining shows fibrils on the BCR cell surface (C) and csFN puncta between cells deep within the BCR (C') (n=11). Bars, 30 µm.
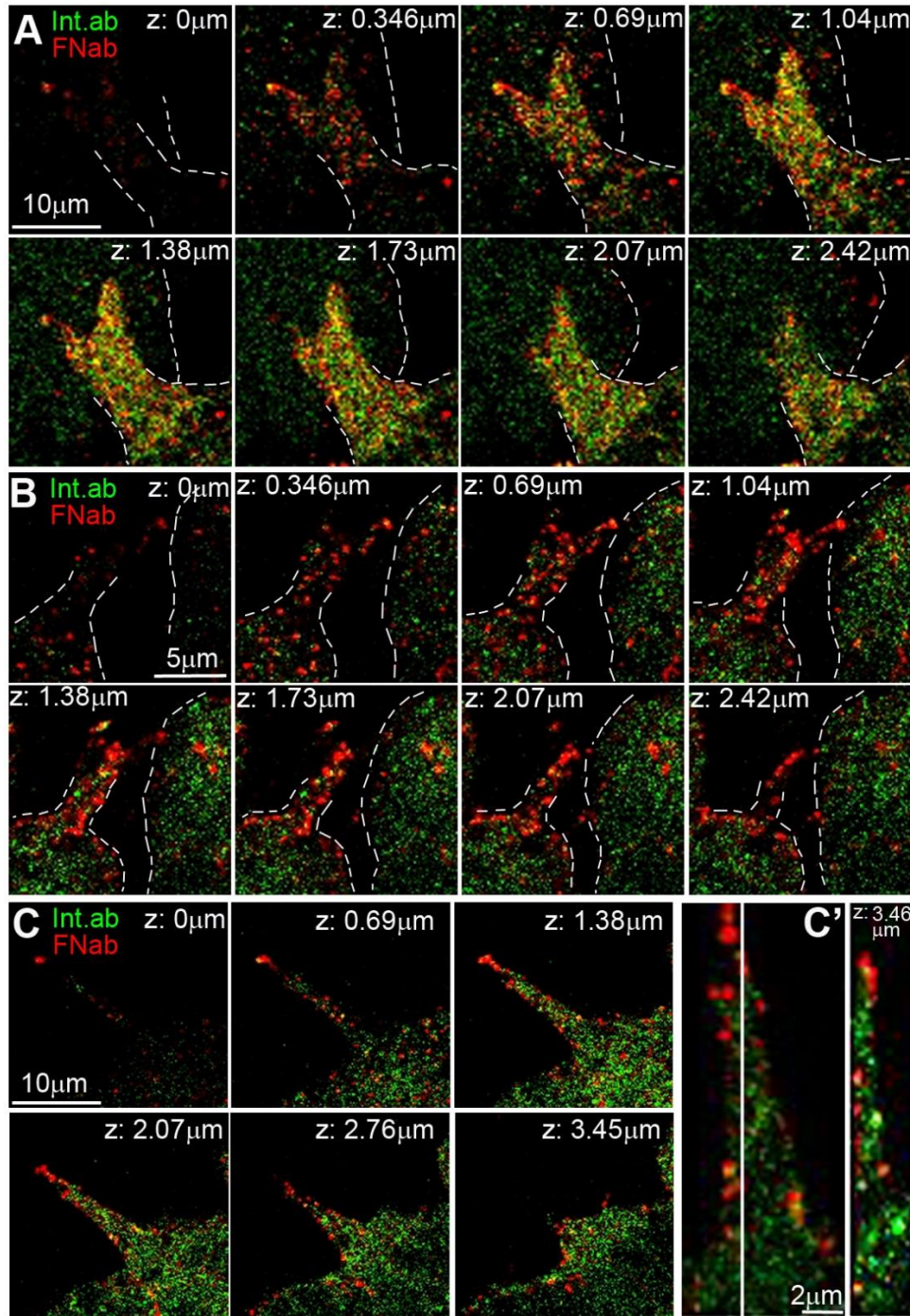
Figure S3. csFN puncta and integrinβ1 on LEM cell protrusions. (A) LEM protrusion on LEM cell surface (see Figure 4F) viewed at different z-planes from free surface to substratum surface. (B,C) LEM cell protrusions over gaps between cells viewed at different z-planes show csFN puncta on all surfaces. (C') z-plane projection. Red, csFN puncta; green, integrinβ1 puncta. (n=22). Dashed lines outline cell bodies.
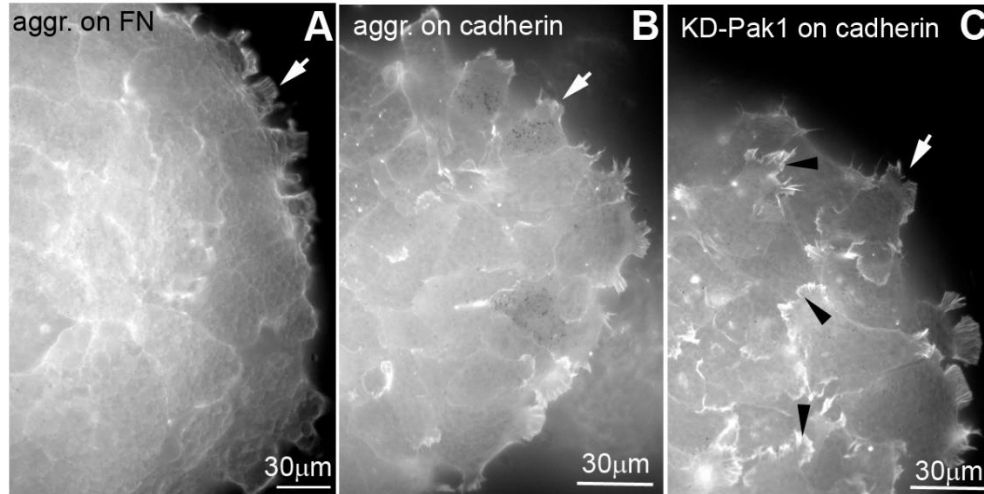
Figure S4. LEM cells can form lamellipodia on C-cadherin substratum. (A,B) F-actin staining with fluorescent phalloidin reveals that LEM explants on substratum coated with bovine serum FN (A) (n=8) or with the extracellular domain of C-cadherin (B) (n=2) form lamellipodia at free margin (arrows). (C) When expressing kinase-dead Pak1, cells form submarginal lamellipodia in addition (arrowheads) (n=3).
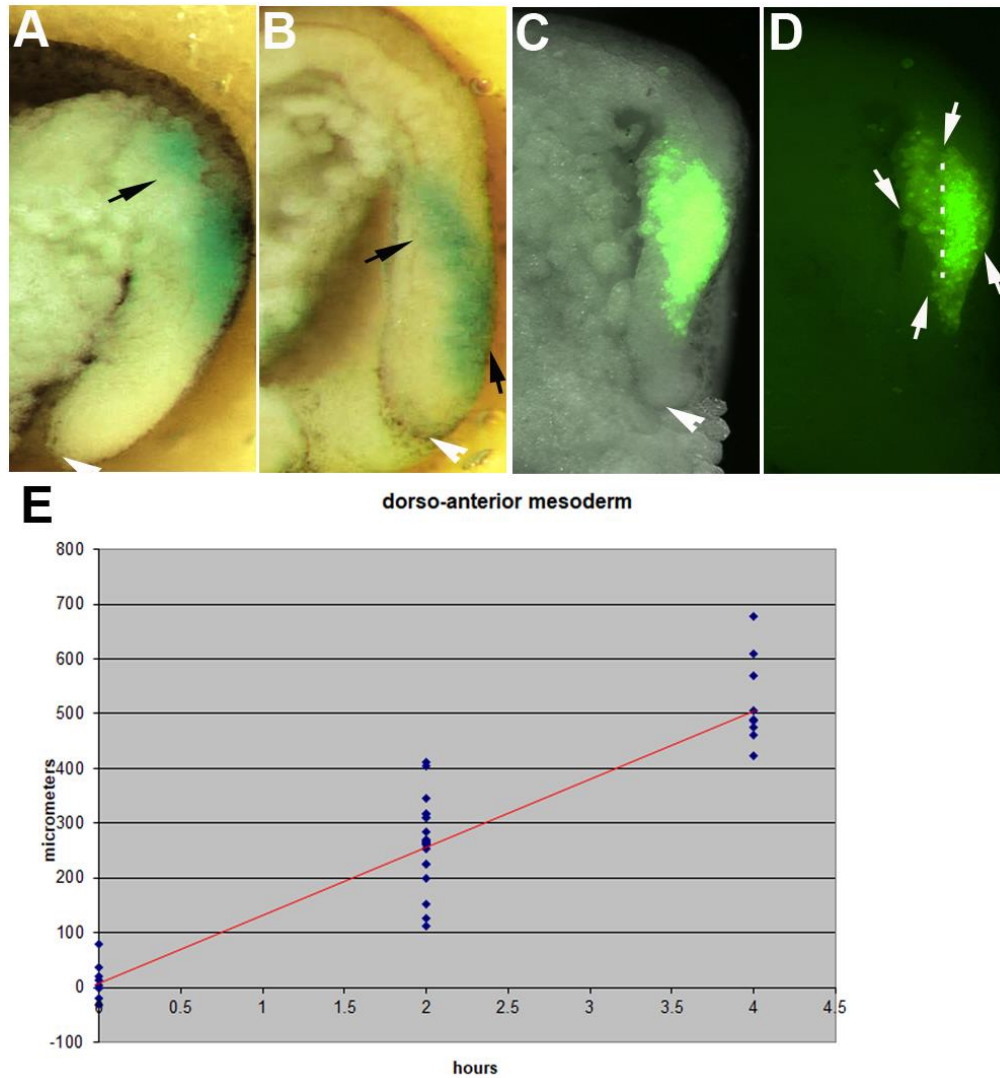
Figure S5. Comparison of LEM and chordamesoderm movements in the gastrula. (A,B) LEM (A) or chordamesoderm (B) were in vivo labeled in register with the overlying BCR by inserting a crystal of nile blue sulfate in the mid-early gastrula. Embryos were fixed after two hours and cut in half mid-sagittally to view the vital stain in mesoderm and BCR (black arrows). (C,D) A plug of BCR and adjacent underlying chordamesoderm was transplanted homotopically from a fluorescein-dextran injected into a non-labeled gastrula. Embryos were fixed after 2 hours and visualized under the fluorescence microscope with (C) or without (D) additional indirect illumination. Dashed line indicates BCR-chordamesoderm boundary. White arrowheads, blastopore. (E) Distances between centers of labeled spots in BCR and LEM were measured for each embryo in specimens fixed after 0, 2 and 4 hours. An average velocity of LEM advance of 2.1 µm/min was calculated from the data (red line).
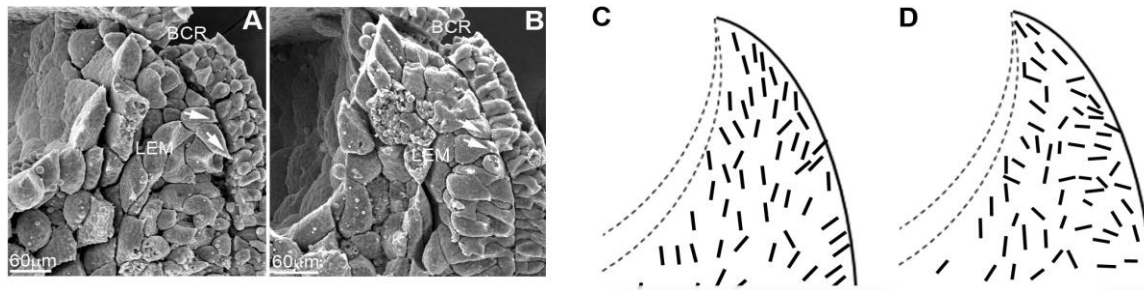
Figure S6. Counter examples to shingle arrangement. (A,B) Two cases were found among 31 scanning electron microscope specimens that showed LEM cells inclined vegetally instead of animally at the BCR-apposed surface in sagittal fractures. (C,D) Cell long axes in the LEM as seen in scanning electron micrographs in the majority of cases (samples from 3 embryos combined) (C) and from the two exceptional cases found with counter-shingle arrangement, combined (D).
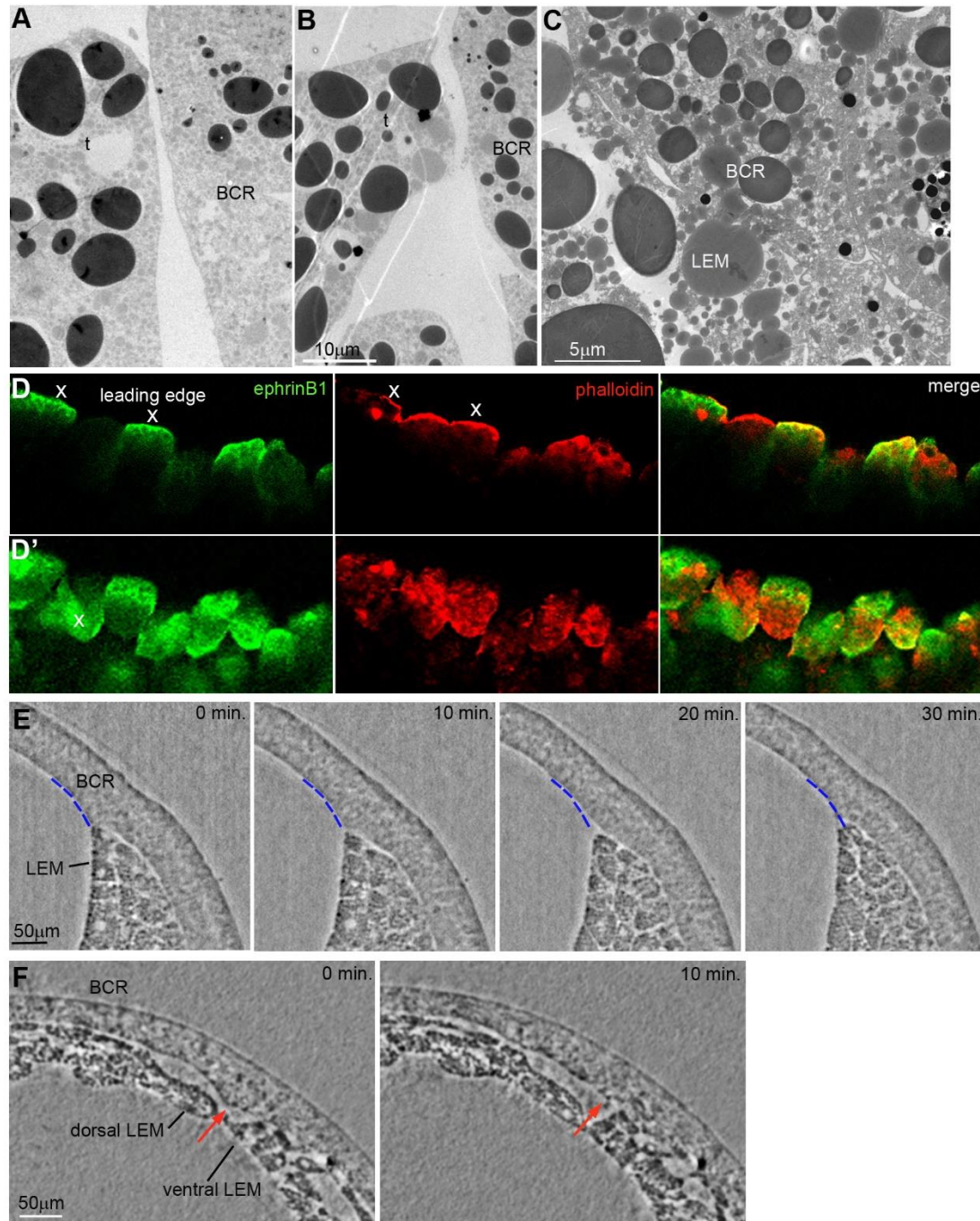
Figure S7. Tip cell characteristics. (A,B) Tip cells (t) can contact the BCR not only through close contacts, as shown in Figure 7G,H, but also through wide contacts, similarly to the contact types seen in LEM lamellipodia-LEM cell surface interactions (n=12). (C) Intimate contact between LEM and BCR cells behind tip during attachment phase (n=24). (D,D') Staining the margin of fixed and excised mid-gastrula LEM with antibody (green) reveals that LEM cells express

ephrinB1, but co-staining for F-actin with fluorescent phalloidin (red) and focussing at different planes (D,D') shows that ephrinB1 is alternatingly enriched at the very leading edge of the tip cells (x) and behind in the cell body (x). (E,F) TXPCµT analysis of BCR cusp retraction. (E) Middle gastrula stage. BCR surface up to cusp apex before transient tip cell detachment (blue dashed line) is indicated at later time points to show degree of cusp retraction. (F) Late gastrula. Black arrows, dorsal and ventral tip cells of LEM meet and detach from BCR cusp (position indicated by red arrow). Retraction by 15 µm (E) or 25 µm (F) takes at most 10 min, i.e. retraction velocities are larger than 1.5 – 2.5 µm/min.
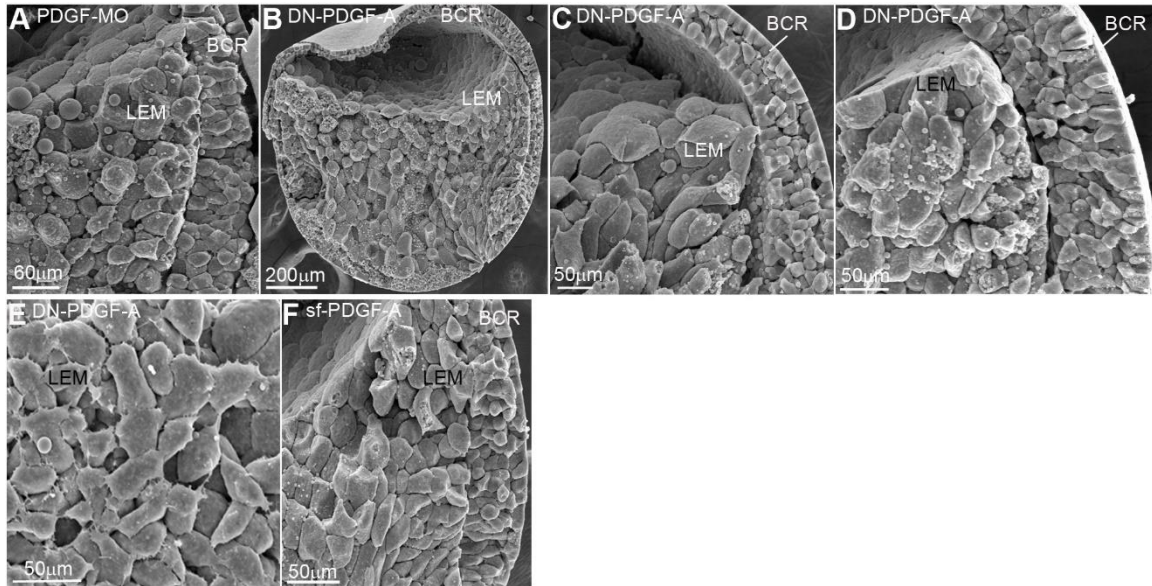
Figure S8. LEM phenotypes after interference with PDGF-A signaling. (A) Knock-down of PDGF-A with MO in the BCR (n=8; 2 experiments). (B-E) Expression of dominant-negative PDGF-A in the BCR. In 10 out of 11 cases, no BCR cusp was present at the position of the LEM tip (n=21; 4 experiments). (F) Overexpression of sf-PDGF-A (n=12; 2 experiments). Sagittal fracturs (A-D,F) and view from the BCR side (E) are shown.

Supplementary Material - **Supplementary Table**

Table S1. Extent of LEM-BCR contacts

A. Scanning electron micrographs (n = 31 embryos)

	front of LEM			rear of LEM			total		
contact	close	mixed	separate	close	mixed	separate	close	mixed	separate
fraction	**0.35**	**0.13**	**0.52**	**0.61**	**0.13**	**0.26**	**0.26**	**0.55**	**0.19**
expected							0.21	0.65	0.14

B. TXPCμT movie (n = 27 frames from 3 different planes of same embryo)

	front of LEM			rear of LEM			total		
contact	close	mixed	separate	close	mixed	separate	close	mixed	separate
fraction	**0.44**	**0.26**	**0.30**	**0.41**	**0.41**	**0.19**	**0.33**	**0.48**	**0.19**
episodes	2.3	1.3	1.7	1.7	2.0	1.7	1.3	2.0	1.7
duration (min)	15.3	16.0	14.1	19.3	16.4	8.9	21.0	19.3	9.0

C. Spatial and temporal distribution of contacts
Semi-quantitative description: close contact = 1; separate = 0; mixed = 0.5

front of LEM	time	0	10	20	30	40	50	60	70	80
	plane 312	0	0.5	0	0	1	0	0.5	0.5	1
	350	0	1	1	1	0.5	0.5	0.5	1	1
	380	1	0	0	0	1	1	0.5	1	1
rear of LEM	312	0	1	1	1	1	0	0.5	1	0.5
	350	0.5	0.5	0.5	0.5	0.5	0	1	1	1
	380	0.5	0.5	0	0.5	1	0	0.5	1	1
average front			0.4	0.4	0.3	0.6	0.7	0.5	0.7	0.9
average rear			0.5	0.6	0.6	0.8	0.4	0.3	0.9	0.9
ratio front/rear			0.8	0.7	0.5	0.8	1.8	1.7	0.8	1.0

(A-C) BCR contacts of front region of LEM (large cells behind tip cell, usually 1-3 cells) and rear region (small cells behind front region) were scored as close (all cells in contact with BCR), separate (none in contact with BCR), and mixed. (A) Scanning electron micrographs (good spatial resolution, no time dimension) and (B,C) a TXPCμT movie (temporal resolution 10 minutes, spatial resolution ca. 1 µm) were used to score contacts. In (A,B) fraction of respective contact types are indicated in bold. In (A) the score for the whole LEM (front plus rear region) are also indicated and compared to the fractions expected from the combinations of the separately scored regions. In (B) successive frames in a given plane showing the same score (0, 1 or 0.5) were counted as "episodes" and averaged over the three planes, and from the total filming time of 80 minutes, the duration of episodes was estimated. In (C) values of 1, 0.5 and 0 were assigned to close, mixed and separate contacts, respectively, determined at 9 time points and at 3 different planes, to calculate averages for front and rear regions for pairs of consecutive frames.